SAPIENZA
UNIVERSITÀ DI ROMA

PhD course

INNOVATION IN IMMUNO-MEDIATED AND HEMATOLOGICAL DISORDERS

XXXV cycle

NON-INVASIVE MINIMAL RESIDUAL DISEASE (MRD) ANALYSIS IN DIFFUSE LARGE B-CELL LYMPHOMA (DLBCL)

Curriculum: Hematology

Department of Translational and Precision Medicine, Sapienza University

Roberta Soscia

Tutor

Prof. Ilaria Del Giudice

AY 2019-2020

CONTENTS

INTRODUCTION

Lymphomas represent a heterogeneous group of malignancies that arise from B or T lymphocytes or natural killer (NK) cells, transformed at different stages of maturation. Lymphomas are classified in macro-groups, Hodgkin's lymphomas (HL), aggressive non-Hodgkin's lymphomas (NHL) and indolent NHL, each with different biological and clinical features as well as therapeutic approaches.
The histological classification of lymphomas is far more complex and has greatly evolved over the years with the accumulation of the knowledge on single lymphomas entities. Indeed, NHL comprise more than 30 subtypes, each with different epidemiology, etiology, immunophenotypic, genetic, clinical features, and response to therapy.
In the Western world, NHL constitute about 80% of all lymphomas. About 85–90% of NHL derive from B cells, whereas the remaining derive from T cells or NK cells. The more frequent forms are diffuse large B-cell lymphoma (DLBCL) and follicular lymphoma (FL) (Sapkota & Shaikh, 2022; Armitage *et al*, 2017; Zelenetz *et al*, 2011).

1. DIFFUSE LARGE B-CELL LYMPHOMA

DLBCL, with estimated 150,000 new cases annually worldwide, represent the most prevalent B-cell NHL (B-NHL) in the adults, representing about one third of NHL in the Western world and 30% to 40% of all new lymphoma diagnoses. It includes cases that arise *de novo* and cases that result from the histologic transformation of indolent B-NHL (i.e., FL and chronic lymphocytic leukemia [CLL]) (Armitage *et al*, 2017; Pasqualucci *et al*, 2015).
The median age at diagnosis of DLBCL is in the mid-60s; 30% of patients are older than 75 years of age. Epidemiologic studies support complex and multifactorial causes of DLBCL, with risk factors including genetic features and immune dysregulation, as well as viral, environmental, or occupational exposures (Cerhan *et al*, 2014).
The number of DLBCL cases in the United States (US) is projected to increase from 29,108 to 32,443 and from 26,078 to 27,981 in Western Europe (WE) from 2020 to 2025, with a total increase rate of 11% in the US compared to 7% in the WE. This increase is also related to the increase in the underlying patient populations with older age groups having higher incidence rates (Kanas *et al*, 2022).
DLBCL itself comprises a heterogeneous group of biologically distinct entities resulting in the clonal proliferation of a malignant B-cell in the germinal center (GC) or post-GC. GCs are highly dynamic structures where mature B-cells undergo rapid proliferation and iterative rounds of somatic hypermutation (SHM), affinity maturation and clonal selection, as well as class switch recombination

(CSR), with the aim of favoring the emergence of cells that produce antibodies with increased affinity for the antigen and capable of distinct effects or functions (Pasqualucci *et al*, 2015).
The disease is aggressive, and the diagnosis is commonly made by the biopsy of a suspicious lymph node or an extranodal site, where the normal architecture is replaced by sheets of large cells that stain positive for pan-B cell antigens, such as CD20 and CD79a.

2. CLASSIFICATION

The clinical and biological heterogeneity of DLBCL has been known to pathologists, molecular scientists and clinicians for decades. Over the last two decades, multidisciplinary efforts allowed to identify unique DLBCL subtypes by either cell of origin (COO) or molecular characteristics. Current classifications of B cell lymphomas are indeed based on multiple parameters, such as morphology, immunophenotype and genetic aberrations (Alaggio *et al*, 2022).
These classification systems are now routinely used to identify subsets of patients with high-risk disease and poorer outcomes to up-front standard R-CHOP (rituximab, cyclophosphamide, vincristine, doxorubicin, prednisone) therapy (Susanibar-Adaniya & Barta, 2021).

CELL OF ORIGIN

It was the introduction of gene expression profiling (GEP) technologies that allowed the formal recognition of multiple distinct subtypes, reflecting either the derivation from discrete B-cell differentiation stages or the coordinated expression of specific transcriptional signatures.
According to the current taxonomy for DLBCL and based on resemblance to the transcriptional profiles of their presumed COO, two main molecular subgroups have been recognized within this diagnostic entity: GC B-cell–like (GCB) DLBCL and activated B-cell–like (ABC) DLBCL, with 10%–15% of cases declared “unclassified”. GCB and ABC subgroups are distinguished by the differential expression of hundreds of different genes, and these genes relate each subgroup to a separate stage of B-cell differentiation and activation.
ABC-DLBCLs are currently thought to be derived from B-cells that have passed through the GC and are committed to plasmablastic differentiation. In contrast, GCB-DLBCLs are postulated to originate from light-zone GC B-cells.
GCB DLBCL have a gene expression profile characteristic of normal GC B-cells with intraclonal heterogeneity, ongoing SHM, CD10 and BCL6 expression.

Conversely, the GEP of ABC DLBCL resembles that of post-germinal or activated B-cells with high expression and constitutive activity of the nuclear factor kappa B (NF-KB) complex and expression of IRF4 and BCL2.

Moreover, while patients with GCB show an overall favorable prognosis, the ABC subtype is characterized by increased aggressiveness and has been associated with a less favorable disease outcome (Pasqualucci *et al*, 2015; Alizadeh *et al*, 2000; Rosenwald *et al*, 2002; Basso & Dalla-Favera, 2015). The COO is determined by the expression of a panel of genes by the nanostring technology, although some immunohistochemistry (IHC) markers can approximate the molecular classification (Hans algorithm) (Hans *et al*, 2004).

MOLECULAR FEATURES

C-MYC is a proto-oncogene located at chromosome 8q24. Ten to 15% of patients with newly diagnosed DLBCL have an underlying MYC rearrangement, identified by fluorescent in-situ hybridization (FISH) (Rosenwald *et al*, 2019). Approximately half of these cases also carry a rearrangement of the anti-apoptotic proto-oncogene BCL2 and/or its transcription repressor BCL6. Their presence defines a DLBCL subset known as double-hit or triple-hit lymphoma, recognized in the 2016 WHO classification as high-grade B-cell lymphoma (HGBCL-DH/TH) (Swerdlow *et al*, 2016). Also, DLBCL can be defined as double expressor lymphoma (DEL) if characterized by overexpression of the c-MYC and BCL2 proteins detected by IHC (≥40% and > 50%, respectively). DELs account for approximately a third of de novo cases and have an intermediate prognosis. DELs can also be detected in up to 50% of relapsed/refractory DLBCL, also associated with poorer outcomes with salvage chemotherapy treatment (Savage *et al*, 2009). Notably, GCB is enriched for DH/TH subtypes and ABC for DEL (Nowakowski *et al*, 2015).

GENETIC SUBTYPES

While recurrent genetic aberrations in individual genes have elucidated oncogenic mechanisms in DLBCL, progresses toward a genetic classification of DLBCL tumors have required the integration of genomic data from multiple analytic platforms to identify genes that were recurrently altered by mutations, translocations, and/or copy-number alterations. Mathematically distinct clustering methods were used to assort DLBCL tumors into genetic subtypes that are characterized by genomic aberrations in subtype-specific hallmark genes.

Schmitz et al. analyzed 574 pre-treatment DLBCL biopsy samples and identified four prominent genetic subtypes each distinguished by genetic aberrations in multiple genes at significantly different frequencies in GCB and ABC cases. These categories include the MCD, BN2, N1, and EZB subtypes.

The MCD subtype was characterized by the co-occurrence of MYD88 (L265P) and CD79B mutations, the BN2 subtype by BCL6 translocations and NOTCH2 mutations, the N1 subtype had frequent NOTCH1 mutations and the EZB subtype had EZH2 mutations and BCL2 translocations. The MCD and N1 subtypes corresponded to ABC disease, while the BN2 and EZB subtypes corresponded to the GCB subtype. These groups differed in responses to immunochemotherapy, with favorable survival in the BN2 and EZB subtypes and inferior outcomes in the MCD and N1 subtypes (Schmitz *et al*, 2018). In parallel, Chapuy and colleagues highlighted the complexity of DLBCLs by classifying 304 primary, previously untreated DLBCLs into five different DLBCL clusters. These include a previously unrecognized group of low-risk ABC DLBCLs of extrafollicular/marginal zone origin; two distinct subsets of GCB DLBCLs with different outcomes and targetable alterations; and an ABC/GCB-independent group with biallelic inactivation of TP53, CDKN2A loss and associated genomic instability (Chapuy *et al*, 2018). Later, Wright and colleagues developed an algorithm called "LymphGen" to provide a probabilistic classification of a tumor from an individual patient into a genetic subtype. They noted that TP53 was the most frequently mutated gene that was significantly enriched not only in one of the previous described subtypes. Tumors with a homozygous TP53 deletion or the combination of a heterozygous TP53 deletion and a TP53 mutation had the highest aneuploidy, therefore they formed a class of cases called A53. They also observed that mutations in TET2, P2RY8, and SGK1 were recurrently mutated among the genetically unassigned cases, leading to the creation of a new class, termed ST2 (Wright *et al*, 2020).

Figure 1 shows the heterogeneous biologic features that reflect the insights gained over the past 20 years.

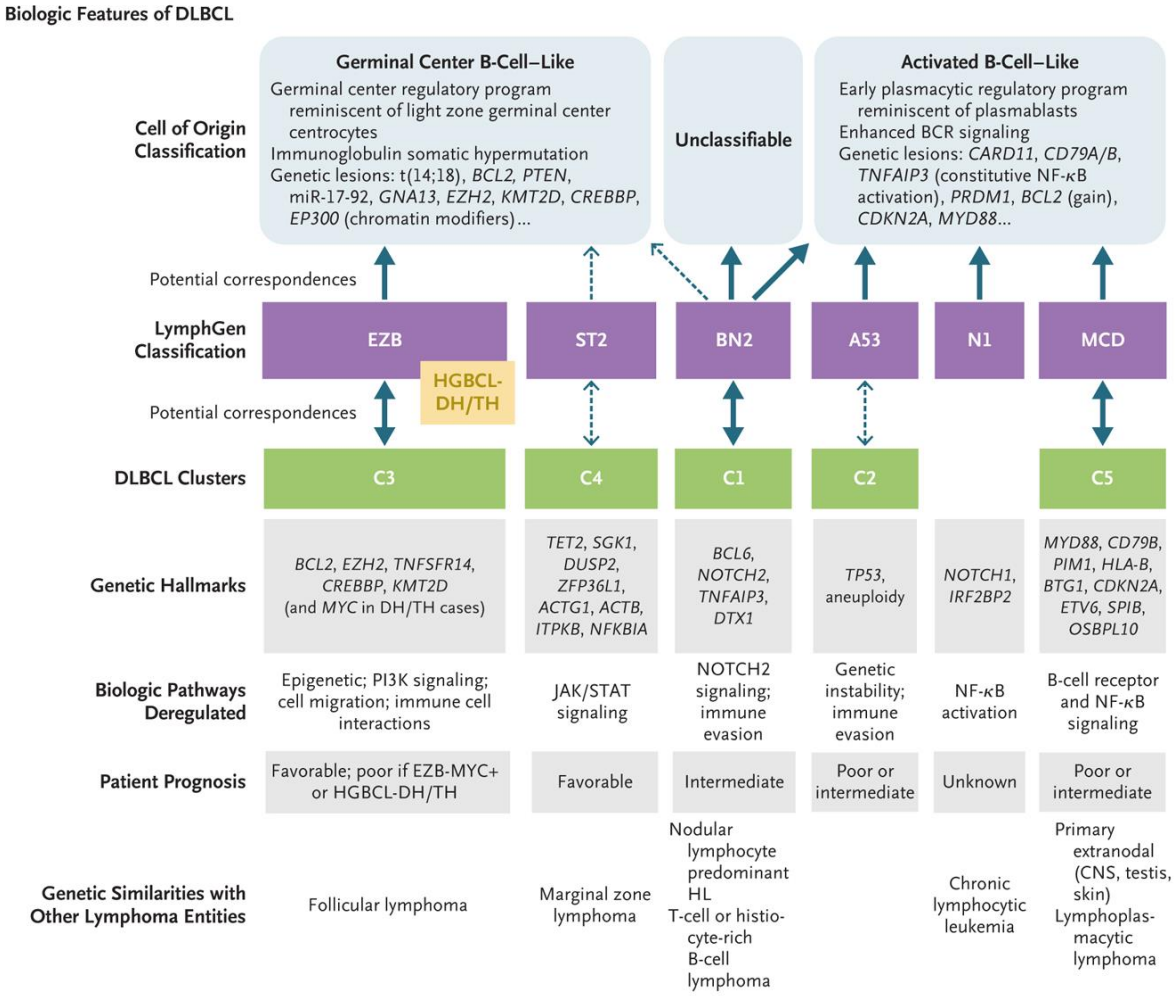

Figure 1. *From Sehn et al, N Engl J Med 2021.*
Solid arrows indicate robust associations, dashed arrows indicate weaker associations or uncertain associations. BCR denotes B-cell receptor, CNS central nervous system, EBV Epstein–Barr virus, HHV8 human herpesvirus 8, HIV human immunodeficiency virus, HL Hodgkin's lymphoma, miR-17–92 microRNA cluster 17–92, NF-κB nuclear factor κB, PI3K phosphatidylinositol 3-kinase, SLE systemic lupus erythematosus, and TNF/LTA, tumor necrosis factor/lymphotoxin alpha.

3. RISK STRATIFICATION

A combination of several prognostic tools to stratify DLBCL patients into risk groups are employed, utilizing clinical, molecular, or radiographic features.

Patients with DLBCL were first shown to be potentially curable with anthracycline-containing polychemotherapy in the mid-1970s (McKelvey *et al*, 1976; Anderson *et al*, 1977; Fisher *et al*, 1993). Since then, the most important advance in the management of DLBCL was the recognition that the addition of the monoclonal anti-CD20 antibody, rituximab, to the CHOP chemotherapy, the so-called R-CHOP regimen, significantly improves the outcome of patients (Sehn *et al*, 2005; Coiffier *et al*, 2010; Tilly *et al*, 2015), with more than 50% of patients with advanced-stage de novo DLBCL being cured (Friedberg *et al*, 2011).

Despite the major advances obtained with immuno-chemotherapy, a relevant number of patients still experience treatment failure, and the time of failure is one of the most important prognostic factors at relapse together with the eligibility or not for autologous stem cell transplantation (ASCT) (Coiffier *et al*, 2010; Gisselbrecht *et al*, 2010; Giné & Sehn, 2016). Indeed, 20% to 50% of patients will be refractory to R-CHOP or will relapse after achieving complete response (CR). Moreover, the current salvage therapy seems to be inadequate in nonresponding patients: only 30% to 35% of resistant or relapsed patients can achieve a prolonged progression-free survival (PFS) with high-dose chemotherapy followed by ASCT in the rituximab era (Gisselbrecht *et al*, 2010).

It is therefore important to promptly identify patients who are unlikely to be cured with first-line immunochemotherapy and develop personalized therapy strategies.

Several prognostic score systems have been established and applied to predict the survival of patients with DLBCL. The International Prognostic Index (IPI) has been widely used since 1993 to predict prognosis in aggressive NHL treated with doxorubicin-containing regimens (International Non-Hodgkin's Lymphoma Prognostic Factors Project, 1993). It is based on age, stage, performance status (PS), lactate dehydrogenase (LDH), extranodal sites.

The IPI has been validated and refined in the rituximab era (R-IPI) and in patients with <60 years of age (age-adjusted IPI) (Ziepert *et al*, 2010). It has also been expanded to include the more granular information about each of these variables in the recent National Comprehensive Cancer Network IPI (NCCN-IPI), allowing greater discrimination among high-risk patients (Zhou *et al*, 2014; Ruppert *et al*, 2020).

However, these clinical indexes have limitations, since they are not able to identify patients at very high risk or to discern biologic heterogeneity; moreover, they are principally based on pretreatment characteristics and do not incorporate information that emerges during treatment (Rushton *et al*, 2020).

Invasive tissue biopsies are the gold standard to obtain, beside the diagnosis, the molecular information that can stratify lymphoma patients for COO and into genetic subgroups.

However, these invasive biopsies do not capture spatial tumor heterogeneity or treatment-emergent clonal evolution (Hav *et al*, 2019; Alizadeh *et al*, 2015). Moreover, tissue biopsies are problematic for several anatomic sites such as the central nervous system and deep abdominal compartments. Therefore, innovative technologies that facilitate the detection, quantification, and characterization of lymphomas in real-time are needed to overcome these limitations, to help a modern prognostic stratification and to support novel strategies of lymphoma precision medicine.

4. STAGING AND RESPONSE ASSESSMENT

At present, staging and response assessment should be performed in accordance with Ann Arbor staging and the Lugano classification criteria (Cheson *et al*, 2014; Barrington *et al*, 2014; Cheson *et al*, 2016). In the recent years, ^{18}F-fluorodeoxyglucose positron-emission tomography with computed tomography (PET/CT) has replaced CT because of its higher sensitivity. End-of-treatment response by PET/CT is interpreted according to the Deauville five-point scale. Moreover, studies evaluating the value of interim PET/CT have yielded conflicting results, with no treatment modification performed solely on the base of interim PET/CT (Barrington *et al*, 2014). Moreover, its use in the assessment of response to therapy has limitations due to false positives results in the setting of concomitant inflammation or infection, or false-negative results due to its inability to detect microscopic disease. These limitations are demonstrated by the mixed results using the Deauville score visual assessment in determining early response to therapy (Mamot *et al*, 2015). Costs and risk of ionizing radiation are the main issues related to an extensive use of imaging techniques.

Thus, limitations of imaging are represented by the following aspects: i) imaging has a relatively low sensitivity in assessing tumor response (Pregno *et al*, 2012); ii) it cannot detect disease at the molecular level or dynamically monitor or identify the biological mechanisms that drive the development of tumors, such as tumor heterogeneity and clonal evolution; iii) it often cannot significantly anticipate tumor relapse respect to the reappearance of clinical signs/symptoms of disease.

5. MINIMAL RESIDUAL DISEASE

Under the definition of minimal residual disease (MRD) are included all methods able to measure a disease below the sensitivity of the conventional tools. Technologies used to evaluate and measure MRD can be nowadays divided into three main categories: (1) those coming from the molecular biology, (2) the flow cytometry, and (3) the imaging.

In the last 20 years many groups around the world focused their research on the evaluation of the MRD, in order to identify a disease recurrence before the time when the “conventional” laboratory or imaging tools can demonstrate it.

MRD molecular techniques have been developed from the classic qualitative and quantitative PCR approaches to the new digital droplet PCR (ddPCR) and the next-generation sequencing (NGS) tools; they have been widely used in a variety of hematological malignancies with a significant circulating cellular component, such as leukemias (Roschewski *et al*, 2022; Lauer *et al*, 2022).

However, MRD in lymphoma is not as established as in leukemia. A sizable group of lymphomas do not show peripheral dissemination of the disease in detectable amount. Circulating tumor cells (CTCs), even if present at diagnosis, become negligible after therapy and confined primarily to inaccessible nodal sites. Therefore, hiding as a source of relapse, residual cells keep multiplying undetected only to re-emerge as a mass visible on imaging scans and later with clinical sign and symptoms.

Most research is moving to improve the cure rate for DLBCL with the development of novel targeted therapies designed to overcome mechanisms of cellular resistance (Roschewski *et al*, 2014). With the emergence of targeted therapies, that will be combined (or even substitute) to immunochemotherapy in NHLs, and could theoretically treat subclinical disease, clinically validated molecular technologies are needed to assess the MRD.

The development of robust techniques, including NGS, together with the discovery of circulating nucleic acids and circulating exosomes, has opened the door to leukemia-like research in NHLs, as advanced molecular methods are more sensitive than imaging in the measurement of residual disease and can do so without radiation exposure.

Recently, the 'liquid biopsy' has emerged as an innovative non- or minimally-invasive approach to detect and characterize cancers, through profiling of tumor-derived analytes in body fluids, most commonly blood but also cerebrospinal fluid (CSF), urine, ascites, pleural fluid, or saliva.

Circulating tumor DNA (ctDNA) has become the most investigated analyte in lymphomas, as the majority of lymphoma patients do not present with circulating disease and therefore, CTCs are usually a less attractive target. ctDNA is shed from tumor into circulation and represents a subset of the total cell-free DNA (cfDNA) pool released into the peripheral blood (PB) after normal physiologic processes of apoptosis, proliferation, and necrosis (Roschewski *et al*, 2016; Rossi *et al*, 2019).

Major advances in molecular techniques have led to an improved detection of minimal ctDNA amounts in body fluids, facilitating ultrasensitive detection of minute residual disease during or after therapy for early identification of treatment failure and prediction of disease relapse in numerous cancer entities including lymphoma.

6. ctDNA-BASED MRD ASSESSMENT BY GENE MUTATIONS

Because of the genomic intra-tumor heterogeneity, with different areas or sites of the same lymphoma showing different mutations, a single tissue biopsy might not be representative of the entire tumor genetics and may miss subclones residing in anatomically distant sites. Therefore, ctDNA can be used as a non-invasive tool to track recurrently mutated genes in DLBCL, allowing to capture the

mutational landscape beyond the intra-tumoral heterogeneity (i.e., liquid biopsy), to monitor the disease after treatment and to detect the emergence of treatment-resistant clones and therefore the clonal evolution of the disease (Rossi *et al*, 2017).

The utility of liquid biopsy requires an adequate sensitivity and specificity to detect minute amounts of ctDNA in body fluids. The choice of liquid biopsy technique depends on which application is of interest. Both PCR-based (mainly ddPCR) and NGS-based methods have been applied to analyze lymphoma-related mutations in ctDNA.

ddPCR allows the quantification of single, hotspot genomic variants, with a 10−5 detection limit and a relatively low cost, but it has the disadvantage of screening a limited number of mutations.

NGS techniques, with the ability to screen a wide range of genetic aberrations with high sensitivity, have recently proved a powerful tool for ctDNA identification. Targeted amplicon-based or hybrid-capture NGS technologies allow to study hundreds of lymphoma-specific genetic regions, covering the entire spectrum of recurrent genetic alterations. In this regard, the cancer personalized profiling by deep sequencing (CAPP-seq) technology currently represents one of the most sensitive assay.

The comparison of sequencing results obtained from ctDNA and the initial tumor biopsy is highly useful to discriminate variants that are present at a very low allele frequency from the background noise, particularly for monitoring the residual disease (Lauer *et al*, 2022; Huet & Salles, 2020).

Recently, the Stanford group further improved the deep sequencing of ctDNA by developing an innovative approach that further maximizes the analytical sensitivity and reduces the background error rates by tracking two or more variants (‘phased variants’) on the same strand of one single DNA molecule (‘PhasED-seq’, Phased Variant Enrichment and Detection Sequencing). This method offers extremely low error profiles while maintaining high genome recovery, thus facilitating ctDNA monitoring down to an analytical detection limit of ~0.00005% (i.e., 1 in 2,000,000). PhasED-seq seems particularly useful in B-cell lymphomas, as mutations accumulate in stereotyped genetic regions caused by the ongoing and aberrant SHM through the activity of the enzyme activation-induced cytidine deaminase (AID) (Kurtz *et al*, 2021). A similar strategy has been recently employed by Meriranta and colleagues, providing additional evidence that tracking of phased variants can significantly improve the sensitivity of ctDNA detection in lymphoma patients (Meriranta *et al*, 2022).

7. ctDNA-BASED MRD ASSESSMENT BY IMMUNOGLOBULIN REARRANGEMENTS

B-cell lymphoid malignancies are the progeny of a B-cell clone characterized by a unique footprint of clonal immunoglobulin (*IG*) gene rearrangements, that serve as a diagnostic marker for clonality assessment. Patient-specific primers targeting the clonal rearrangement of the *IG* gene locus can be designed for virtually all patients, although this method remains too labor intensive to be used in clinical practice. Alternatively, clonal rearrangement of the *IG* genes can be identified on the initial tumor tissue using a single NGS assay that uses universal primers for all possible rearrangements. The specific clonotype of each patient can be subsequently tracked for disease monitoring.

The first paper demonstrating that plasma could be the best compartment for MRD assessment in aggressive lymphomas was published in 2015: the *IG* heavy chain (*IGH*) and *IG* light chain (*IGK*) clonalities were tested by the LymphoSIGHT technology in 105 tumor samples, and in 83% of them it was possible to find a molecular marker. Interestingly, a disease-specific molecular marker was identified in plasma in a higher percentage of cases than in the PB mononuclear cells, and the molecular disease resulted twice higher in plasma. At the time of progression/relapse, all patients were MRD-positive in the plasma while only 30% of them showed tumor cells circulating in the PB (Kurtz *et al*, 2015). More recently, the same group reported a strict correlation between the cfDNA levels and the response to therapy: in patients where cfDNA levels decreased of 2-logs after one cycle (=early molecular response, EMR) and of 2.5-logs after two cycles of chemo-immunotherapy (=major molecular response, MMR), the event-free survival (EFS) was significantly longer than that observed in cases with a lower molecular disease reduction. In multivariate analysis, including IPI and interim PET, MRD still retained its independent prognostic value (Kurtz *et al*, 2018). However, EMR and MMR still misclassified certain patients at these fixed time points. Thus, the authors developed a dynamic approach integrating various prognostic factors measured before and during treatment (i.e., IPI, pretreatment ctDNA, COO, EMR, MMR, and interim PET/CT) into one single algorithm that dynamically updates the patient's risk over time as long as more information becomes available (Continuous Individualized Risk Index, CIRI). This personalized method was applied to an independent validation cohort and outperformed conventional risk factors such as IPI, COO, interim PET/CT, and even EMR and MMR, for outcome prediction (Kurtz *et al*, 2019).

In another early study by Roschewski *et al.*, the level of ctDNA measured by *IG* high-throughput sequencing was assessed after each cycle of first-line therapy, and patients without detectable ctDNA after two cycles had a superior five-year PFS compared with patients who remained ctDNA positive (Roschewski *et al*, 2015).

In line with these observations, other studies have investigated the role of ctDNA for monitoring DLBCL after treatment and for detecting early molecular relapse (Scherer *et al*, 2016), also in other

therapeutic settings. For example, Hossain and colleagues for the first time assessed the MRD by ctDNA in 6 patients receiving the anti-CD19 chimeric antigen receptor (CAR) T cell therapy (CAR-T) for relapsed/refractory (rr) DLBCL. The "molecular" MRD after day +28 was compared to the MRD assessed by PET: in four out of five cases the increased values of ctDNA preceded progression before PET, and all progressing patients had increasing ctDNA when PET confirmed the clinical progression, thus supporting the idea that the MRD when assessed in the plasma could be the most important predictive tool of the DLBCL patients' outcome (Hossain *et al*, 2019).

Two major recent studies evaluated the role of ctDNA in DLBCL patients who were treated with CAR T-cell therapy in more detail. Frank et al. used IgHTS to detect V(D)J clonotypes in the plasma of 72 rrDLBCL patients undergoing treatment with axicabtagene ciloleucel (axi-cel). They found that 70% of patients responding to CART-cell therapy had undetectable ctDNA 7 days after infusion, compared to 13% of progressing patients. At multiple time points after axi-cel infusion (days 21, 28, and 56), ctDNA positivity was predictive of clinical outcomes (Frank *et al*, 2021). In another study, Sworder et al. used CAPP-Seq to profile ctDNA before and after axi-cel therapy. They demonstrated that ctDNA levels were prognostic for PFS in univariate analyses both at diagnosis and at several time points after CAR T-cell infusion (Sworder *et al*, 2021).

Similarly, Merryman et al. applied IgHTS to 141 patients with rrDLBCL undergoing ASCT and found that the identification of ctDNA in the apheresis stem cell samples was predictive of PFS and OS (Merryman *et al*, 2020).

Although not yet entered into the clinical practice, the non-invasive quantification of tumor burden and the MRD monitoring during and after treatment is becoming the most established application of ctDNA in DLBCL (Poynton & Okosun, 2021; Cirillo *et al*, 2020; Melani *et al*, 2019; Huet & Salles 2020; Lakhotia & Roschewski 2021).

8. IMMUNOGLOBULIN GENE REARRANGEMENTS MONITORING

To perform MRD analysis, it is necessary to identify *ab initio* a molecular marker that will be followed during or after treatment: in general, for B-cell lymphomas, rearrangements of *IGH* or *IG* light chains (kappa or lambda, *IGk, IG*λ) can be used. Indeed, the first molecular technique for MRD assessment in DLBCL to be published used the principle of *IG* rearrangements (Jiang *et al*, 2015).

Since lymphomas originate from the malignant transformation of individual lymphoid cells, all lymphomas generally share one or more cell-specific or "clonal" antigen receptor gene rearrangements. Therefore, clonality assessment is based on this feature. In patients suspected for having a B-cell lymphoma, clonality assessment enables the demonstration of a clonal expansion of

clonally related B cells, all having the identical molecular footprint of the antigen receptor encoded by the *IG* genes. These clonotypes can be identified in tumor tissue and monitored in cfDNA over time.

The *IGH* gene locus on chromosome 14 (14q32.3) includes 46-52 functional and 30 non-functional variable (VH) gene segments, 27 functional diversity (DH) gene segments, and 6 functional joining (JH) gene segments spread over 1250 kilobases. The *IGH* gene consists of three highly variable complementary determining regions and three rather conserved framework regions (FR), interspersed among each other. The antigen-binding site, known as CDR3, is the most variable region of the rearranged *IGH* gene.

The proper assembly of a functional B-cell receptor (BCR) is controlled by several checkpoints at different stages of B-cell development (Rajewsky, 1996). Once a mature B cell has encountered an antigen, it will undergo SHM in the GC. The BCR is generated by a stepwise process involving rearrangements of the different germline variable (V), diversity (D), and joining (J) *IG* genes, called V(D)J recombination. This process is initiated by the recombination-activating gene (RAG) products RAG1 and RAG2, which relies on the recognition of recombination signal sequences (RSSs) flanking the individual genes (Gellert, 2002). V(D)J recombination starts with the *IGH* chain by the recombination of one of the D genes with one of the J genes, followed by the subsequent joining of one of the V genes to the rearranged DJ gene (Figure 2).

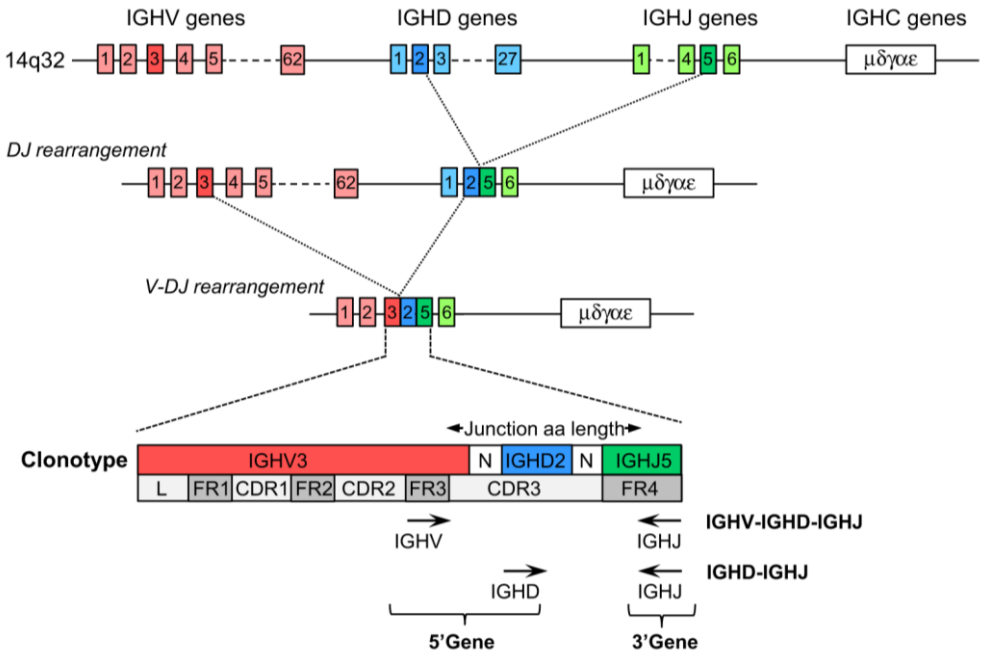

Figure 2. *Adapted from Scheijen et al, Leukemia 2019.*

For the light chain (*IGK* or *IGL*), a direct V to J gene rearrangement takes place, where the *IGK* locus will first undergo gene rearrangement. When there is no productive *IGKV- IGKJ* rearrangement, additional rearrangements will occur that inactivate the *IGK* locus by removal of the *IGKC* region and the enhancers. These rearrangements involve the kappa deleting element (*KDE)* sequence that can rearrange to one of the kappa V genes and thereby delete the initial *IGKV- IGKJ* rearrangement, resulting in an *IGKV-KDE* rearrangement or to an isolated RSS that is located in the J kappa-C kappa intron (intron *RSS- IRSS*), resulting in an *IRSS-KDE* rearrangement. If there is no proper *IGK* rearrangement, the *IGL* genes will rearrange. When B cells fail or become autoreactive during this process, they will be silenced and eliminated. B cells that assembled a functional BCR will further diversify by undergoing SHM to extend the *IG* repertoire upon antigen recognition within the GC of a lymph node. During this process, random sequence alterations are introduced to improve antigen binding, a phenomenon called affinity maturation. Coupled to transcription, SHM occurs within a small defined (1.5−2 kb) region of DNA and is initiated from the transcriptional promoter 300bp upstream of each rearranged V segment; the process is terminated immediately downstream of the involved J segment. These point mutations occur over the entire length of the V-D-J exon of the *IGH* genes and the V-J exon of the *IGK* and *IGL* genes.

AIMS OF THE STUDY

DLBCL is a heterogeneous disease with striking genetic diversity and variable outcomes. Treatment response assessment relies on CT and PET/CT scans, which cannot detect disease at the microscopic level. ctDNA is an emerging biomarker that overcomes the fundamental limitations of imaging scans and the invasiveness of tissue biopsies. It can measure the effectiveness of treatment by detecting the presence of MRD any time during the course of the disease. In order to improve the cure rate of DLBCL patients, the clinical development of molecular monitoring tools capable of early detection of treatment failure and disease relapse is warranted. PB monitoring of tumor-specific molecules represents a paradigm shift in the way of assessing tumor response and relapse prediction in DLBCL.

The present study is based on the analysis of PB samples and formalin-fixed, paraffin embedded (FFPE) diagnostic lymph node biopsies in a large cohort of patients with newly diagnosed DLBCL treated with immunochemotherapy. The aims are to:

I) test *IGH* and *IGK* chain gene rearrangements as target of clonality using NGS in FFPE diagnostic lymph node biopsies and ctDNA extracted from PB;

II) explore if tracking clonal *IGH*/*IGK* rearrangements by NGS can be a non-invasive way to study MRD in longitudinal ctDNA samples during/after treatment;

III) study the correlation with radiologic disease assessment of early and final response (CT and PET/CT) and with several clinical variables.

The focus of this thesis is to describe how ctDNA might enhance DLBCL treatment response assessment and outcome prediction thanks to the faceable monitoring of MRD, highlighting its potential use as a decision-making tool to guide lymphoma treatment in the future.

MATERIALS AND METHODS

1. STUDY DESIGN AND PATIENTS

A multicenter cohort of 53 consecutive newly diagnosed DLBCL (27 from Rome and 26 from Novara), aged >18 years, was included in this prospective study. The following biological specimens were collected and analyzed from patients from Rome: diagnostic FFPE lymph node biopsy (for genomic DNA, gDNA) and 30 ml of PB (for cfDNA) before the start of treatment, after 3 cycles of treatment (interim), at the end of treatment, during the follow-up (month +6, +12, +24), and at the time of progression. Regarding the Novara cohort, patients were studied at diagnosis and at the interim time point.

Early (mid-treatment) and final (end of treatment) disease response were assessed by CT and PET/CT, respectively. Patients provided written informed consent, and the institutional review board approved the protocol.

Patients' characteristics are summarized in Table 1. Twenty-eight men and 25 women, diagnosed between 2015 and 2021, with a median age at diagnosis of 63.9 years (range, 19–84). Nine patients were in stage 1, 14 in stage 2, 13 in stage 3, and 17 in stage 4. Patients were followed after R-CHOP or R-CHOP-like chemotherapies.

Table 1. *Patients' characteristics.*

	Rome cohort (n = 27)	**Novara cohort (n = 26)**	**Entire cohort (n = 53)**	***p* value**
Average age (years)	60	61.7	60.8	0.8
Male, n (%)	16 (59.3)	12 (46.2)	28 (52.8)	0.26
Female, n (%)	11 (40.7)	14 (53.8)	25 (47.2)	
Stage, n (%)				
1	5 (18.5)	4 (15.4)	9 (17)	0.23
2	7 (25.9)	7 (26.9)	14 (26.4)	
3	9 (33.3)	4 (15.4)	13 (24.5)	
4	6 (22.2)	11 (42.3)	17 (32.1)	
IPI, n (%)				
0 to 1	12 (44.4)	8 (30.8)	20 (37.7)	0.34
2	7 (25.9)	6 (23.1)	13 (24.5)	
3	3 (11.1)	7 (26.9)	10 (18.9)	
4 to 5	5 (18.5)	5 (19.2)	10 (18.9)	
LDH elevated, n (%)	13 (48)	12 (46.2)	25 (47)	1

2. gDNA COLLECTION AND EXTRACTION

All FFPE diagnostic tissue derived from excisional biopsies or needle biopsies from lymph nodes. All samples were sectioned in 3-4 μm thick sections. gDNA was isolated from FFPE tissue with the automated Maxwell RSC DNA FFPE Kit (Promega, Madison, Wisconsin), according to the manufacturer's instructions.

DNA amounts were assessed using the NanoDrop ND-1000 UV-Vis Spectrophotometer (ThermoFisher, Waltham, Massachusetts). The Specimen Control Size Ladder master mix (Invivoscribe Inc, San Diego, California) was then used to ensure that the quantity and quality of sample DNA was adequate.

3. cfDNA COLLECTION AND EXTRACTION

A total of 123 PB samples were included in the study: 46/123 (37.4%) were diagnostic samples and 77/123 (62.6%) were samples longitudinally collected: 26 (21.1%) from interim, 16 (13%) from the end of treatment, 15 (12.2%) from month +6, 12 (9.8%) from month +12, and 8 (6.5%) from month +24. At progression, occurring at month +6, +12 and +24, 5 samples were evaluated.

Blood (30 ml) was collected in EDTA tubes (Becton Dickinson, Franklin Lakes, New Jersey) and processed immediately to isolate plasma. Tubes were spun at 800 g for 10 min using a refrigerated centrifuge. Plasma was then removed into new 1.5 ml tubes without disturbing the buffy coat and re-spun at 13000 rpm for 10 min using a refrigerated centrifuge to remove cellular debris.

Plasma was stored in 1 ml aliquots at -80°C.

A total of 4 ml of thawed pooled diagnostic plasma per patient was extracted by the Maxwell RSC48 instrument (Promega) with the commercially available cfDNA purification kit "Maxwell RSC LV ccfDNA kit" (Promega), used according to the manufacturer's instructions (summarized in Table 2). Isolated cfDNA was stored at -20°C until analysis.

DETERMINATION OF QUANTITY AND QUALITY OF cfDNA

Quantification of cfDNA was performed using the Qubit Fluorometer 3.0 (Thermo Fisher) in combination with the Qubit dsDNA HS Assay Kit (Invitrogen, Life Technologies, Carlsbad, California). As per manufacturer's instructions, a standard curve was prepared using the zero and 10 ng/μl Qubit DNA standards provided in the kit. For all cfDNA extractions, 2 μl of each sample were diluted in 198 μl Qubit working solution prior to measurement. Following the volume used for cfDNA elution for each protocol, quantitative measurements of cfDNA were expressed as the total mass of cfDNA (ng) present in the elution volume (75 μl) of the extraction protocol. cfDNA purity (as referred

to absence of gDNA contamination) was established by capillary electrophoresis using an Agilent 2100 Bioanalyzer (Agilent Technologies Inc., Santa Clara, California) equipped with the Expert 2100 software, in combination with a high sensitivity (HS) DNA microchip and HS DNA kit (Agilent Technologies). The assay was performed according to the instructions provided by the manufacturer.

Table 2. *cfDNA extraction method.*

	Maxwell RSC LV ccfDNA kit
Prepare sample	3 ml of plasma 3 ml of Binding Buffer 140 µl of resin
Bind cfDNA	The samples were put in rotation for 45 min and then loaded in the cartridges
Elution step	75 µl of Elution Buffer

4. MOLECULAR ANALYSIS

DETECTION OF CLONAL GENE REARRANGEMENTS BY NGS ANALYSIS OF gDNA

The LymphoTrack *IGH* FR1/2/3 panel (Invivoscribe) was used for the analysis of diagnostic samples aiming to detect clonotypic rearrangements and to identify the DNA sequence specific for each clonal gene rearrangement. Selected cases without a detectable index clonal sequence by *IGH*-targeted testing were also tested using *IGK* primers (Invivoscribe).

Each assay has a single multiplex master mix that targets conserved regions in the *IGH* or *IGK* genes. The LymphoTrack *IGH* FR1/2/3 assay uses primers targeting the *IG* framework regions (FR) to amplify *V(D)J* rearrangements. Each single FR multiplex master mix for *IGH* contains forward primers targeting one of the conserved framework regions (FR1, FR2, or FR3) as well as several consensus reverse primers targeting the JH region. Targeting all three framework regions significantly reduces the risk of not being able to detect the presence of clonality, as somatic hypermutations in the primer binding sites of the involved *VH* gene segments can impede DNA amplification.

The LymphoTrack *IGK* assay contains forward primers targeting conserved *VK* region and intron sequences, with reverse primers targeting *JK* and *KDE* regions.

Identification of clonal sequences follows a three-step workflow (Figure 3, A and B): (1) PCR amplification, (2) NGS and (3) bioinformatics analysis.

In 1-step PCR amplicons are generated and 1-side indexed, allowing the simultaneous sequencing of up to 24 samples in a single run. Each of these 24 indices can be considered to act as a unique barcode

that allows amplicons from individual samples to be pooled together after PCR amplification to generate the sequencing library.

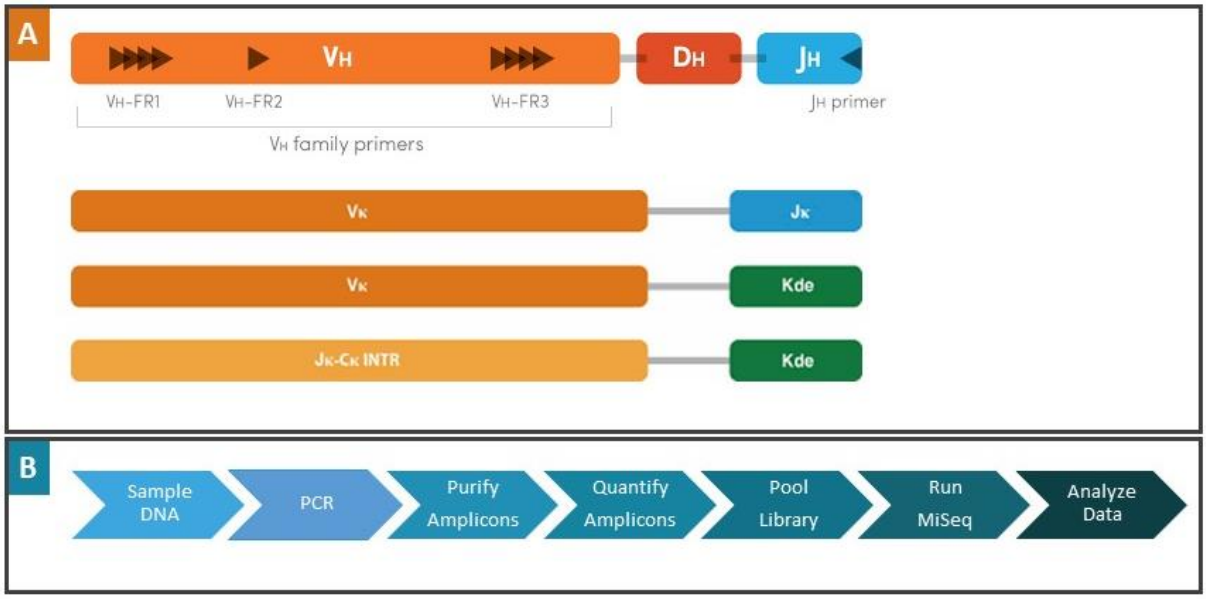

Figure 3. *Overview of the LymphoTrack method.* ***A****, Schematic distribution of consensus primer locations on the IGH and IGK locus.* ***B****, Workflow diagram of assays.*

All baseline samples were sequenced using 150 ng of gDNA. Positive and negative controls for clonality were also included.

PCR amplicons were purified to remove excess primers, nucleotides, salts, and enzymes using the Agentcourt AMPure XP microbeads (Beckman Coulter Inc, Brea, California). This method utilizes solid-phase reversible immobilization (SPRI) paramagnetic bead technology for high-throughput purification of PCR amplicons. Using an optimized buffer, PCR amplicons that are 100 bp or larger are selectively bound to paramagnetic beads while contaminants such as excess primers, primer dimers, salts, and unincorporated dNTPs are washed away. Amplicons were then eluted and separated from the paramagnetic beads resulting in a more purified PCR product for downstream analysis and amplicon quantification. Amplicons purity and quantity were assessed using the KAPA Library Quantification Kits for Illumina platforms (KAPA Biosystems, Boston, Massachusetts). Purified and diluted PCR amplicons and a set of six pre-diluted DNA standards were amplified by qPCR methods, using the KAPA SYBR FAST qPCR Master Mix. The primers in the KAPA kit target Illumina P5 and P7 flow cell adapter oligo sequences.

The average Ct score for the pre-diluted DNA Standards were plotted against $\log_{10}$ to generate a standard curve, which was then used to calculate the concentration (nM) of the PCR amplicons derived from sample DNA. Calculating the concentration of PCR amplicons allowed equal amplicon

representation in the final pooled library. Amplicons generated with this LymphoTrack master mixes were prepared between 12 and 20 pM. These libraries were later sequenced in a MiSeq instrument (Illumina, San Diego, California) using the MiSeq Reagent Kit v2 (500-cycle) with 2×251 bp length, aiming at achieving 1 million reads per sample.

Specifically, the amplified products in the library are hybridized to oligonucleotides on a flow cell and are amplified to form local clonal colonies (bridge amplification). Four types of reversible terminator bases (RT-bases) are added, and the sequencing strand of DNA is extended one nucleotide at a time. To record the incorporation of nucleotides, a CCD camera takes an image of the light emitted when fluorescently labeled nucleotides are added to the sequencing strand. A terminal 3' blocker is added after each cycle of the sequencing process and any unincorporated nucleotides are removed prior to the addition of four new RT-bases (Figure 4).

The primer sets contain barcoded sequence adaptors, allowing demultiplexing of reads after sequencing on Illumina MiSeq instruments (Illumina).

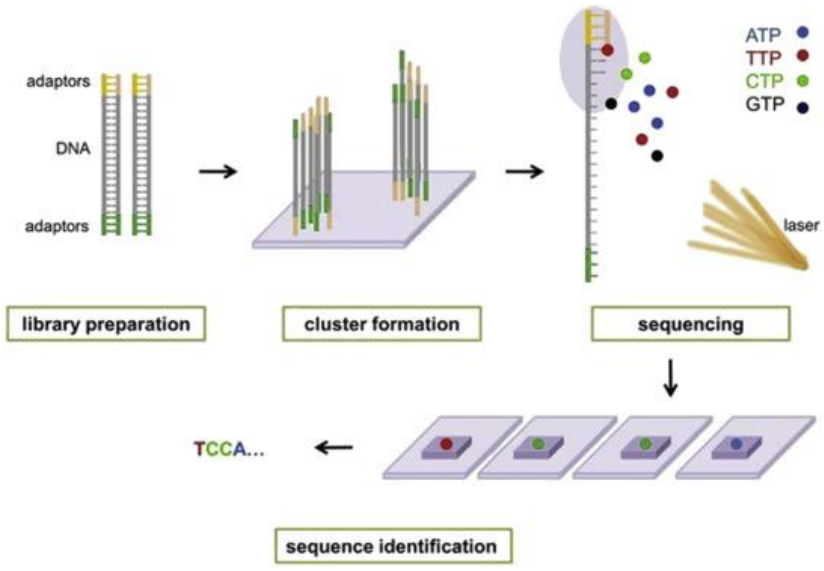

***Figure 4**. An overview of Illumina sequencing.*

SEQUENCE ANALYSIS OF TUMOR BIOPSIES AND CLONALITY ASSESSMENT

After demultiplexing, bioinformatics analysis was done by processing FASTQ files, generated during NGS, with the LymphoTrack Software-MiSeq v2.4.3 (Invivoscribe) to retrieve sequences from virtually every clonal B-cell in the samples. Tumor associated-clones at diagnosis were identified following 3 criteria: (1) 20,000 or more total reads for each sample; (2) at least 1 but not more than 2 merged top reads with 2.5% or greater (for *IGH*) and 5.0% or greater (for *IGK*) of total reads; and (3) top first or second merged reads at least two times more abundant than the third most abundant read to be considered clonotypic (for *IGH*), top first or second merged reads at least two times more

abundant than the fifth most frequent merged sequence if there is at least ore *INTR-Kde* rearrangement detected in the four most frequent merged sequences or the third if there are no *INTR-Kde* detected (for *IGK*). The result of each assay was called as clonal, non-clonal or indeterminate (i.e., too few reads for evaluation) (Figure 5, A and B).

Clonotype frequencies within a sample were determined by calculating the number of sequencing reads for each clonotype divided by the total number of passed sequencing reads in the sample.

Data from the run were considered invalid if either the % cluster passing filter or the % base calls above Q30 (%>Q30) were below 75%.

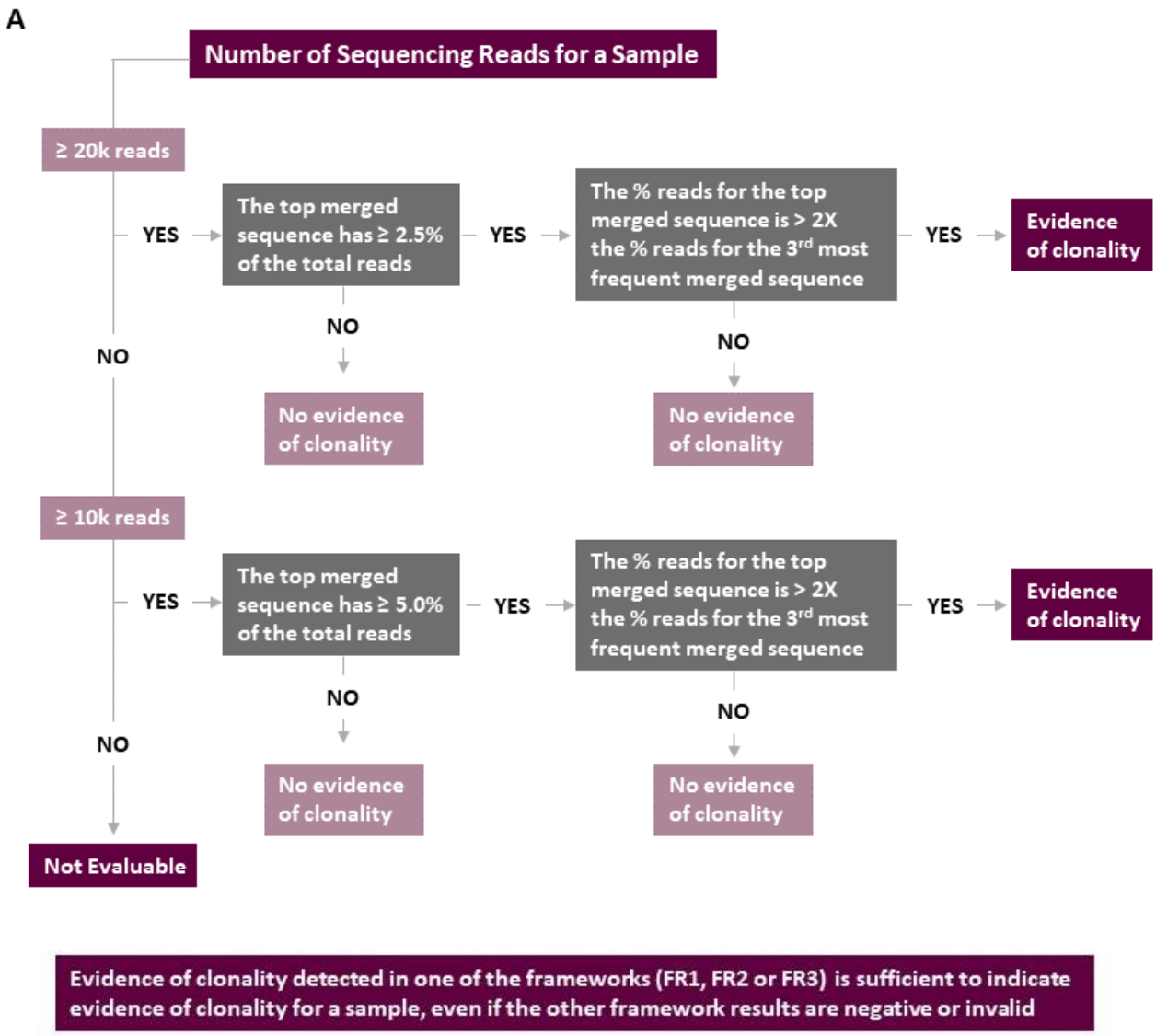

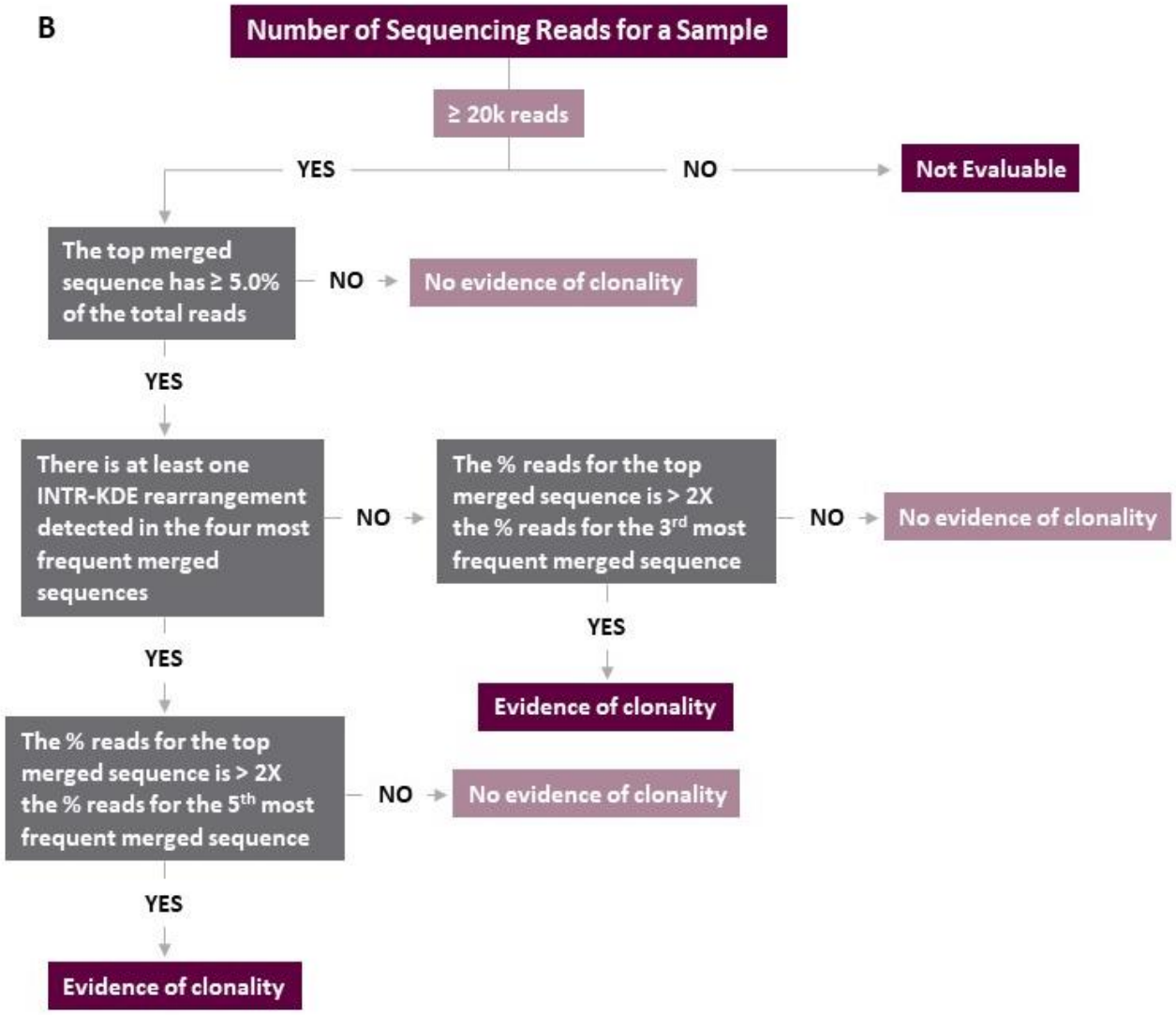

***Figure 5. A**, IGH FR1/2/3 clonality assessment flowchart and **B**, IGK clonality assessment flowchart.*

DETECTION OF CLONAL GENE REARRANGEMENTS BY NGS OF ctDNA

The lymphoma-derived sequences identified in biopsies were used as a target to assess the presence of molecular disease on serial plasma samples on ctDNA.

The LymphoTrack *IGH* FR2/3 (FR1 multiplex master mixes were excluded due to the small fragment size of cfDNA of ~166 bp) and LymphoTrack *IGK* assay panels (Invivoscribe) were used to assess MRD following similar methods as described above. Testing was done using only the primer sets that successfully characterized the diagnostic clone.

To maximize the probability to detect clonality in ctDNA samples, testing was performed in quadruplicate reactions using the maximum amount of ctDNA allowed by the protocol (10 µl). A PCR replicate was defined as an independent PCR amplification with a unique LymphoTrack master

mix (index); indeed, different indexes were used between replicates of the same sample. To avoid cross-contamination during sequencing, monitoring samples from the same patient were sequenced in different runs, using different barcode indexes. Moreover, a rotation instrument schedule was instituted so samples from the same patient would not be sequenced within 2 runs of each other, performing a sodium-hypochlorite post-run wash on the instrument to reduce carry-over contamination.

A no-template control and a low positive control (MRD level =1,00x10^{-4}) were also included in every run.

Libraries generated with this LymphoTrack master mixes were later sequenced in a MiSeq instrument (Illumina) using the MiSeq Reagent Kit v2 (500-cycle) with 2×251 bp length. A total of eight replicates from two patients were pooled together with the low positive control aiming for >1 million reads per sample.

SEQUENCE ANALYSIS OF PLASMA SAMPLES

The FASTQ files were analyzed using the LymphoTrack Software-MiSeq v2.4.3 (Invivoscribe). MRD was then calculated with the bioinformatics tool LymphoTrack MRD Software v2.0.2 (Invivoscribe) considering the number of replicates, the amount of DNA (ng) for each replicate, the "*Unique Reads"* file generated with the LymphoTrack Software-MiSeq v2.4.3 (Invivoscribe) and the number of total reads. The MRD Software generates an "*output.tsv*" file with the full analysis of each sequence and a PDF report with the MRD results for each PCR replicate analyzed.

For an "MRD Detected" result, the software reports the number of reads and cumulative frequencies of exact matched sequences and similar sequences (up to two mismatched nucleotides). For an "MRD Not Detected" result, the software reports the number of reads and cumulative frequencies of exact matched sequences and similar sequences (up to two mismatched nucleotides). In addition, the software reports the confidence level at 10^{-3}, 10^{-4}, 10^{-5} and 10^{-6} sensitivity for the reached sequence based upon sample's DNA input and read depth obtained.

Sequencing results were considered invalid when fewer than 20.000 total reads were retrieved.

5. STATISTICS

Comparisons between clinical variables and clonotype frequencies on lymph node and ctDNA were performed by Mann-Whitney and Student *t* test. Pearson correlation was used to compare LDH levels, and a Chi-square test was performed to correlate ctDNA clonotype identification with disease stage.

A ROC curve was created to plot the sensitivity and specificity of both the clonotype frequencies on lymph node and on plasma with a threshold of 50%.

Survival probabilities were estimated using the Kaplan-Meier method; the log-rank test was used to determine the significance of the difference between Kaplan-Meier curves. Two survival end points were considered: PFS, where an event was defined as progression or relapse, and overall survival (OS), where an event was defined as death resulting from any cause. Regression analysis of multiple covariates was conducted by Cox proportional hazards modeling. All p-values were two-tailed. Statistical analyses were carried out using SPSS Statistics v.27.0 (IBM Corp., Armonk, NY).

RESULTS

1. PATIENTS' POPULATION

A prospective series of 53 consecutive untreated DLBCL patients were enrolled and followed after R-CHOP or R-CHOP-like chemotherapies.

Overall, two patients showed refractory disease, 10 had a relapse after a median of 17 months from the start of treatment (range 9–29). After a median follow-up of 37 months (range 2–59), 41 patients remained disease-free.

The refractory patients died during treatment, 7 patients died for disease progression after relapse, 2 died of causes unrelated to lymphoma.

2. IDENTIFICATION OF CLONOTYPIC IMMUNOGLOBULIN REARRANGEMENTS IN PATHOLOGIC SPECIMENS

Tumor biopsies were evaluable in 52/53 patients; in one case, the diagnostic biopsy sample had insufficient quality and quantity of DNA and was excluded from the study.

A total of 52 diagnostic biopsies were tested with a combination of FR1, FR2 and FR3 primer sets. At least one dominant tumor-specific clonotype was identified in 88.5% (46 of 52) of patients with sufficient amount of amplifiable DNA. Nine of the 46 patients had clonal sequences that were only detectable by *IGK* primers (Figure 6). In the remaining 6 cases (11.5%), both *IGH* and *IGK* clonality assessment showed polyclonal patterns and an index clone was not identified; in these cases with undetectable clonality, DNA was also suboptimal in terms of quantity and quality (highly fragmented). Total read counts averaged 370,090 (range, 10,376 to 1,604,541).

Of all 46 patients with a tumor-specific clonotype, most cases (63%, 29/46) were successfully characterized by one assay (1 for *IGH*-FR1, 10 for *IGH*-FR2, 9 for *IGH*-FR3, and 9 for *IGK*); eleven (24%) specimens were clonal for two assays (10 for *IGH*-FR2/3, and 1 for *IGH*-FR1/2); and six (13%) specimens were clonal for all three *IGH* assays (FR1/2/3). Table 3 summarizes the cumulative detection of *IGH* and *IGK* rearrangements. The average length of the sequenced fragments was: 300 bp for FR1, 250 bp for FR2, 100 bp for FR3. Overall, the usage of all primer sets extremely increased the clonality detection rate (Figure 7). Of the 46 cases successfully characterized, 39 (85%) showed one distinct clonal sequence, four cases (9%) showed two unrelated clonal sequences (likely biallelic) with different *IGH* and *IGK* V-J gene segment usages (Figure 8A), whereas three cases (6%) showed two identical *IGH* V-J segment usage but varying in sequence by ≥ 2bp (Figure 8B).

Compared with the reference germline sequence, most index clones showed high somatic hypermutation rates, with a median rate of 7.4% (range, 0.0% to 35.8%).

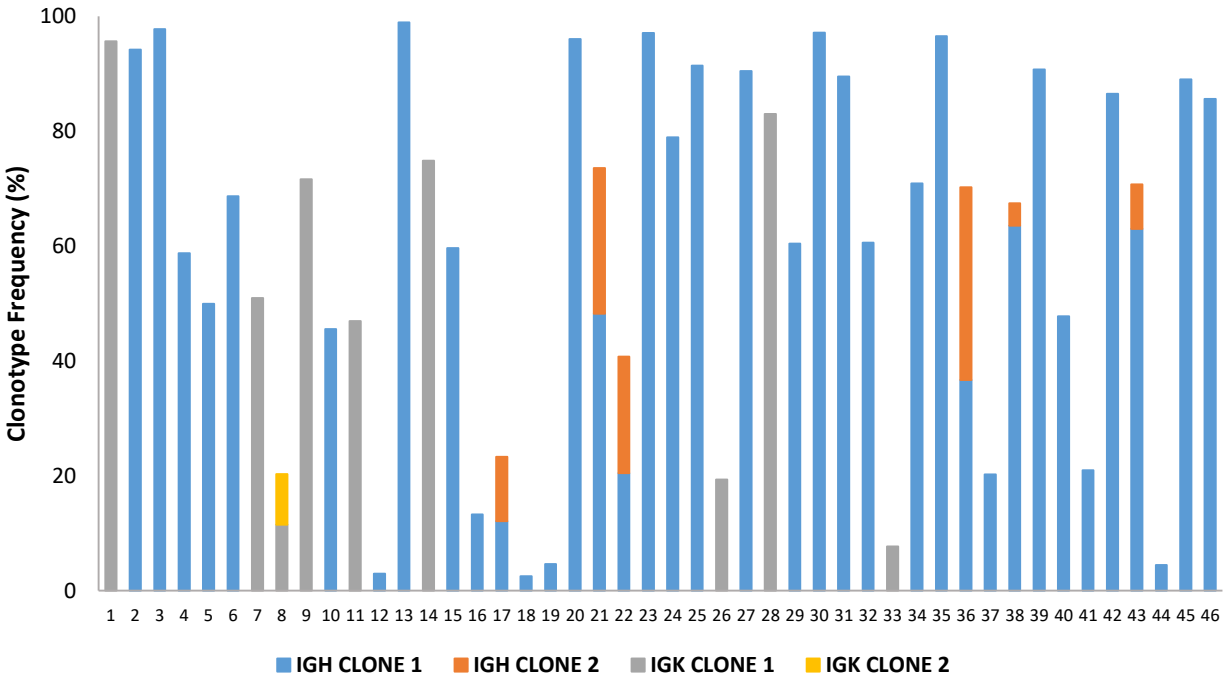

Figure 6. *Comparison of number and burden of clonal IGH and IGK rearrangements. For each patient the number of clones is shown.*

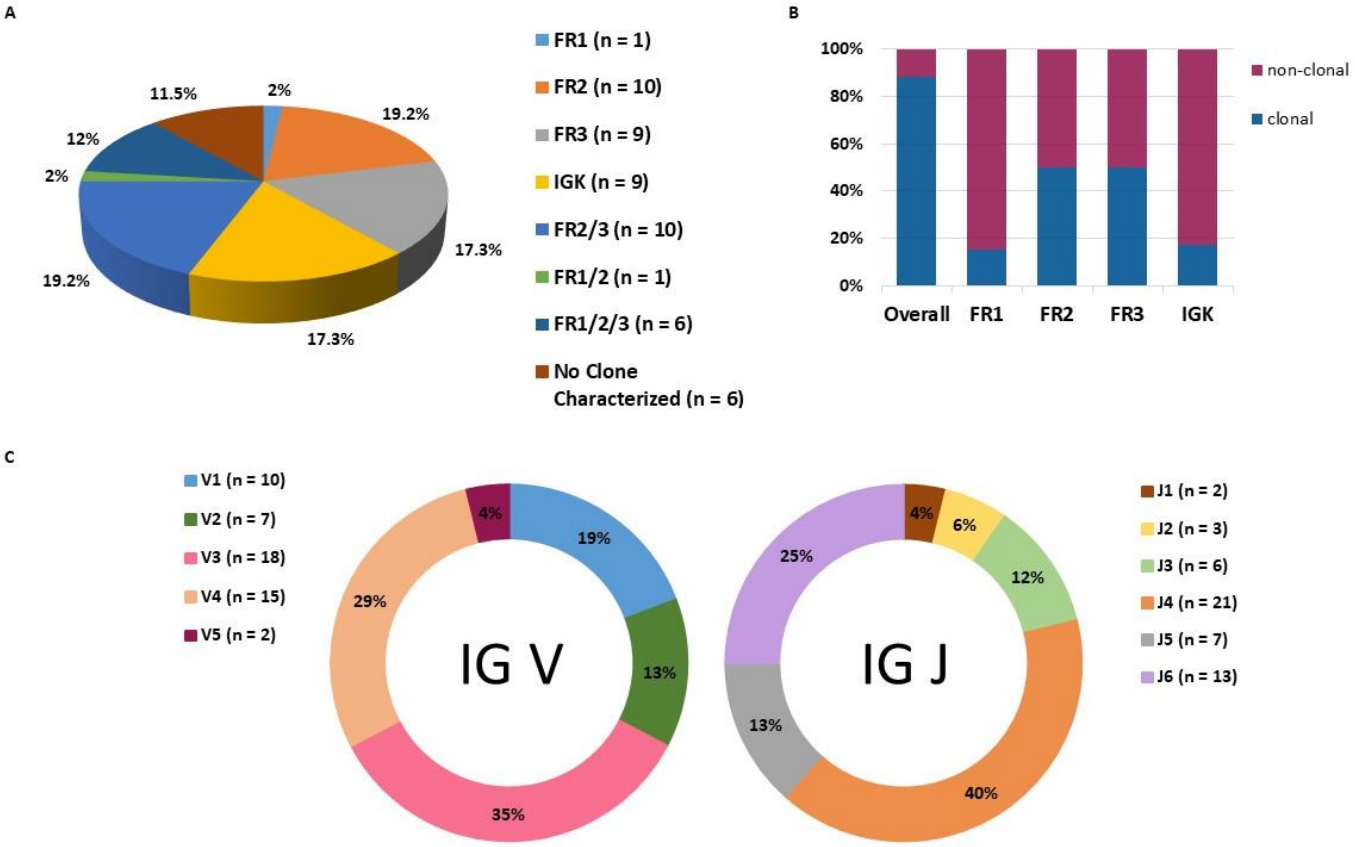

Figure 7. *Characteristics of the clonal sequences:* ***A****, Proportion of cases with clones successfully characterized by each primer sets or by a combination of primer sets or not clonally characterized.* ***B****, Percentage of clonality determination detected by IGH primers (FR1, FR2, FR3 only) and IGK and overall clonality assessment. Note the higher percentage by using all primer sets.* ***C****, IG V and IG J family usage among all the clones identified by IGH and IGK primers.*

Table 3. *IGH and IGK rearrangements found in the diagnostic specimens.*

No	No clone	Assay	Clone1 (%)	Clone2 (%)	Total (%)
ID29	1	IGK	V2D-30*01-J5*01 (95.65)		95.65
ID2	1	FR3	V2-70*11-J4*02 (94.22)		94.22
ID14	1	FR2+FR3	V4-34*02-J4*02 (97.77)		97.77
ID17	1	FR2+FR3	V1-46*02-J4*02 (58.75)		58.75
ID19	1	FR3	V1-1*01-J4*02 (49.97)		49.97
ID21	1	FR2+FR3	V3-48*03-J4*02 (68.68)		68.68
ID22	1	IGK	INTR-Kde (50.97)		50.97
ID57	2	IGK	V2D-29*01-J5*01 (11.48)	V1-27*01-J5*01 (8.84)	20.32
ID53	1	IGK	V2-24*01-J4*01 (71.61)		71.61
ID67	1	FR2	V3-74*03-J4*02 (45.56)		45.56
ID68	1	IGK	V2-29*03-J4*01 (46.96)		46.96
ID79	1	FR2	V5-51*04-J5*02 (2.96)		2.96
ID72	1	FR2+FR3	V4-34*12-J5*02 (98.97)		98.97
ID78	1	IGK	V4-1*01-J4*01 (74.85)		74.85
ID85	1	FR2	V1-2*04-J5*02 (59.67)		59.67
ID86	1	FR2	V4-59*05-J3*01 (13.30)		13.30
ID3	2	FR2	V4-59*08-J3*02 (12.09)	V3-30-3*01-J4*02 (11.22)	23.31
ID6	1	FR2	V3-30*18-J4*02 (2.50)		2.50
ID34	1	FR3	V1-46*01-J6*02 (4.66)		4.66
ID81	1	FR2+FR3	V4-34*01-J6*03 (96.05)		96.05
ID83	2	FR2	V3-49*02-J6*03 (48.25)	V3-49*02-J6*03 (25.33)	73.58
ID84	2	FR3	V4-59*10-J3*02 (20.48)	V5-51*02-J4*02 (20.30)	40.78
ID87	1	FR2+FR3	V4-34*13-J4*02 (97.12)		97.12
ID015	1	FR2	V1-8*01-J6*02 (78.95)		78.95
ID028	1	FR2+FR3	V4-39*02-J6*02 (91.44)		91.44
ID002	1	IGK	V2D-30*01-J2*04 (19.33)		19.33
ID012	1	FR1+FR2+FR3	V3-21*02-J4*02 (90.46)		90.46
ID009	1	IGK	V4-1*01-J2*01 (83.00)		83.00
ID008	1	FR3	V3-72*01-J5*02 (60.42)		60.42
ID007	1	FR2+FR3	V3-35*01-J3*02 (97.14)		97.14
ID027	1	FR2+FR3	V3-48*03-J4*02 (89.54)		89.54
ID025	1	FR2+FR3	V4-61*08-J6*02 (60.58)		60.58
ID003	1	IGK	V4-1*01-J3*01 (7.71)		7.71
ID023	1	FR2	V2-5*08-J4*02 (70.92)		70.92
ID039	1	FR1+FR2+FR3	V3-48*01-J2*01 (96.53)		96.53
ID004	2	FR1+FR2+FR3	V3-30-5*02-J6*02 (36.68)	V3-30-5*02-J6*02 (33.55)	70.23
ID010	1	FR3	V1-2*04-J6*02 (20.25)		20.25
ID030	2	FR1	V3-30-3*02-J1*01 (63.57)	V3-30-3*02-J1*01 (3.86)	67.43
ID021	1	FR1+FR2+FR3	V4-34*13-J3*01 (90.74)		90.74
ID026	1	FR2	V3-33*06-J4*02 (47.77)		47.77
ID031	1	FR1+FR2	V3-66*02-J6*02 (20.99)		20.99
ID016	1	FR1+FR2+FR3	V4-34*02-J4*02 (86.53)		86.53
ID032	2	FR1+FR2+FR3	V1-46*01-J6*02 (63.01)	V4-28*01-J6*02 (7.71)	70.72
ID013	1	FR3	V1-46*01-J4*02 (4.44)		4.44
ID042	1	FR3	V3-49*05-J4*02 (89.00)		89.00
ID043	1	FR3	V1-2*03-J4*02 (85.60)		85.60

A

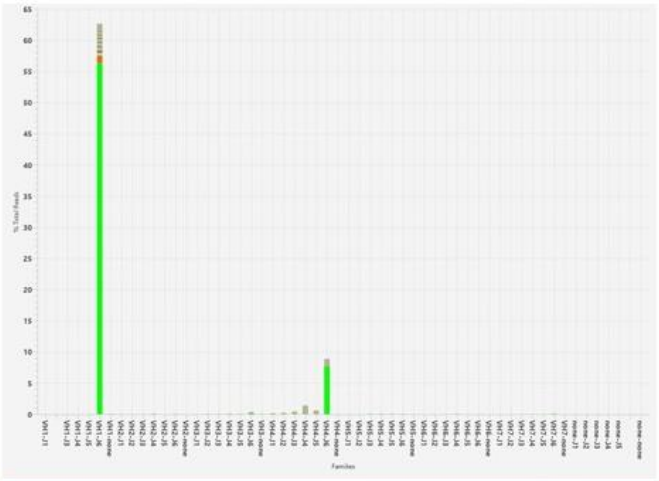

Rank	Sequence	Length	IGH V-gene	IGH J-gene	% total reads	In-frame (Y/N)	No Stop codon (Y/N)	V-coverage
1	TCTGAGGACACC	77	IGHV1/21-1_01	IGHJ6_02	63,01	Y	Y	100,00
2	ACACGGCCATAT	70	IGHV4-28_06	IGHJ6_02	7,71	Y	Y	81,82
3	ACACGGCTGTGT	73	IGHV4-39_01	IGHJ1_01	0,06	Y	Y	93,10
4	ACACGGCCGTG	79	IGHV4/15-8_03	IGHJ3_02	0,05	Y	Y	100,00
5	ACACGGCCGTG	99	IGHV4/15-8_03	IGHJ6_03	0,05	N	N	100,00
6	ACACGGCTGTGT	88	IGHV4-34_13	IGHJ4_02	0,05	Y	Y	100,00
7	ACACGGCTGTAT	79	IGHV4-39_02	IGHJ4_02	0,05	Y	Y	89,66
8	ACACGGCTGTGT	85	IGHV4-39_02	IGHJ3_02	0,05	Y	Y	89,66
9	ACACGGCTGTGT	85	IGHV4-39_02	IGHJ6_03	0,05	Y	Y	93,10
10	ACACGGCTGTGT	79	IGHV4-34_13	IGHJ3_02	0,05	Y	Y	100,00

B

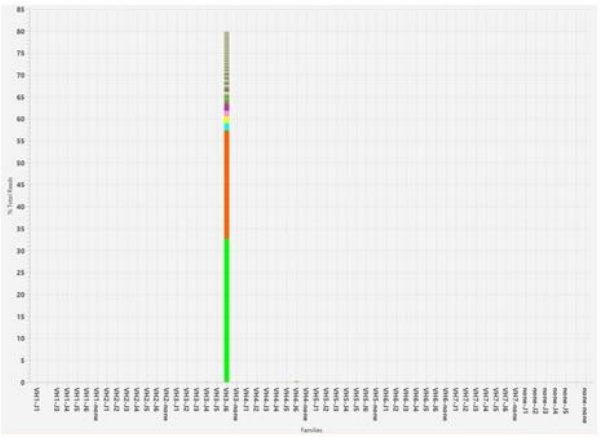

Sequence Alignment

```
1    AGGCAAGGGGCTGGGGTGGGTGACACTTATGC
2    ......................G.........
1    AGTTTGATGGAAGTGATAAATATTATGCAAAG
2    ..................G..............
1    TCCGTGAAGGGCCGATTCACCATCTCCAGAGA
2    ................................
1    CAATTCCAACAACACGATCTATCTGCAAATGA
2    .........G.....A................
1    ACAGCCTGAGACCTGACGACACGGCTGTGTAT
2    ............................C.....
1    TACTGTGCGATTGGCTGGTACAACTATCTTAT
2    ........................G...G....
1    GGACGTCTGGGGCCAAGGGACCAC
2    ..G..............A.....
```

Rank	Sequence	Length	IGH V-gene	IGH J-gene	% total reads	In-frame (Y/N)	No Stop codon (Y/N)	V-coverage
1	AGGCAAGGGGC	216	IGHV3-30_02	IGHJ6_02	48,47	Y	Y	97,70
2	AGGCAAGGGGC	216	IGHV3-30_02	IGHJ6_02	36,25	Y	Y	97,70
3	AGGCAAGGGGC	216	IGHV3-30_18	IGHJ6_02	0,67	Y	Y	97,70
4	TGGCAAGGGGC	216	IGHV3-30_02	IGHJ6_02	0,26	Y	Y	97,13
5	AGGCAAGGGGC	216	IGHV3-30_02	IGHJ6_02	0,15	Y	Y	97,70
6	AGGGAAGGGGC	234	IGHV4-34_02	IGHJ6_02	0,10	Y	Y	100,00
7	AGGCGAGGGTC	216	IGHV3-30_02	IGHJ6_02	0,07	Y	Y	97,70
8	AGGGAAGGGAC	231	IGHV4-61_08	IGHJ6_02	0,06	Y	Y	97,66
9	AGGCAAGGGGC	216	IGHV3-30_02	IGHJ6_02	0,05	Y	Y	97,70
10	AGGGAAGGCCC	222	IGHV2-70_01	IGHJ2_01	0,05	Y	Y	99,41

Figure 8. A*, Example of clonal characterization of tumor biopsy for a case with two unrelated clonal sequences.* ***Bottom panel****: after merging of sequencing reads within 2-bp differences, the sequences are ranked in descending order of % of total IGH sequencing reads. Clonal sequences corresponding to the tumor are highlighted in yellow.* ***Top panel****: the sequences are grouped by IGH V-J gene usages, with each color representing a unique sequence after merging.* ***B****, Example of clonal characterization of tumor biopsy for a case with clonal heterogeneity.* ***Bottom panel****: clonal sequences corresponding to the tumor are highlighted in yellow. A case is considered to have clonal heterogeneity if there are multiple sequences with identical length of PCR products and IGH V-J gene usages, and differences of ≥ 2 bp from each other.* ***Top panel****: the sequences are grouped by IGH V-J gene usages, with each color representing a unique sequence after merging.* ***Right panel****: a comparison of the top two sequences after merging that illustrates clonal heterogeneity is shown. A dot represents an identical nucleotide across the sequences, whereas the differences are highlighted with red bold nucleotides.*

3. BASELINE PLASMA SAMPLES ANALYSIS AND CONCORDANCE WITH TUMOR BIOPSIES

In the 46 patients with tumor-derived *IG* clonotype successfully identified in biopsies, paired pre-treatment PB samples were analyzed to assess the ability of NGS to detect clonality in cfDNA. The mean plasma cfDNA concentration was 26.5 ng/mL (range, 1.9–155). ctDNA clonality was detected in 41 of the 46 (89%) patients. In the group of positive plasma samples, the average and median value of ctDNA were 26.4 and 12.7 ng/mL, respectively (range, 2–155); whereas among negative plasma samples were 7.4 and 4.3 ng/mL, respectively (range, 1.9–14.4).

Thus, higher pretreatment concentrations of cfDNA were associated with a higher rate of clonality detection, possibly because of higher tumor burden (Figure 9).

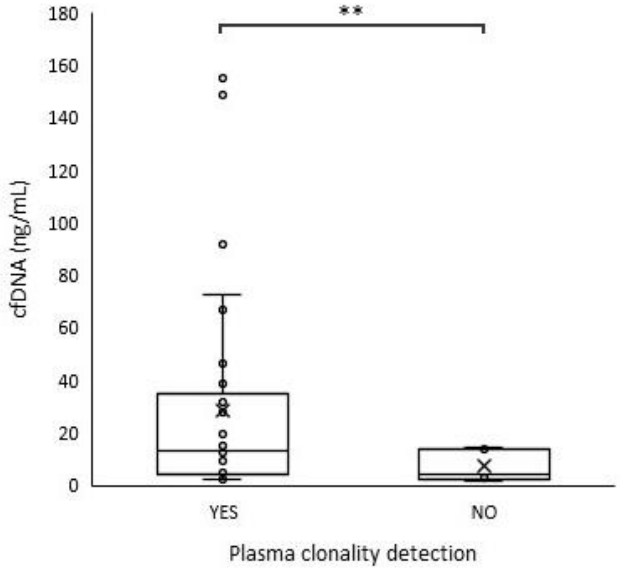

Figure 9. *Boxplot representation of cfDNA amount according to the detection of clonality in the plasma samples.*
***p < 0.01*

The clonal *IG* rearrangements identified in ctDNA at diagnosis were then matched with lymphoma-specific clonotype.

Identical clonality calls between paired samples were found in 33/41 cases, giving an informativity rate of 80.5%. In the remaining 8/41 cases (19.5%), different clonal rearrangements were found in the plasma compared to lymph node.

Total read counts averaged 176,246 (range, 12,164 to 865,923).

Five diagnostic biopsy samples had clonal sequences identified by FR1/2/3 assays, 2/5 ctDNA samples had clonal sequences that were only detectable by FR2, and 3/5 only by FR3. In 3 cases, diagnostic samples were characterized by FR2/3 assays and on ctDNA 2 cases showed clonality by

FR2 assay and the last case only by FR3 assay. Overall, the assays concordance (i.e., FR1, FR2, FR3 or *IGK*) in the clonality detection between lymph node and ctDNA was of 76% (25/33). These results highlight the importance of applying all primer sets to detect clonality in plasma samples.

Figure 10A and B show an example of clonality concordance on the two analyzed compartments.

A

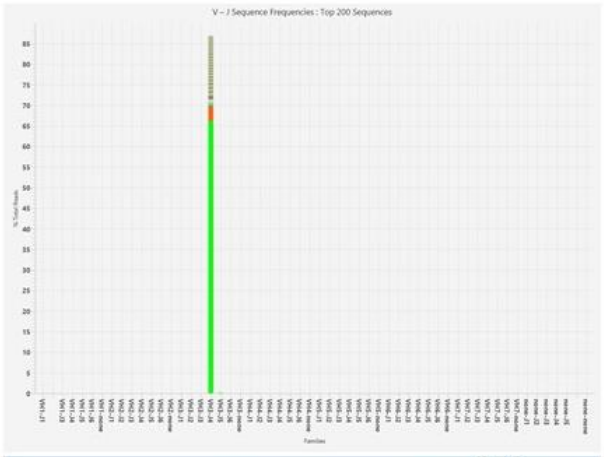

Rank	Sequence	Length	IGH V-gene	IGH J-gene	% total reads	In-frame (Y/N)	No Stop codon (Y/N)	V-coverage
1	AGGGAAGGGG	234	IGHV3-21_02	IGHJ4_02	90,46	Y	Y	99,43
2	TGGATTCAGCTT	282	IGHV3-21_02	IGHJ4_02	0,12	Y	Y	100,00

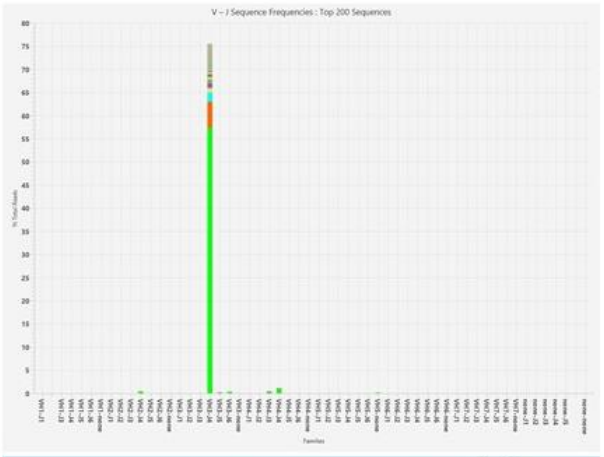

Rank	Sequence	Length	IGH V-gene	IGH J-gene	% total reads	In-frame (Y/N)	No Stop codon (Y/N)	V-coverage
1	AGGGAAGGGG	234	IGHV3-21_02	IGHJ4_02	79,49	Y	Y	99,43
2	AGGGAAGGGA	234	IGHV4-59_08	IGHJ4_02	1,17	Y	Y	100,00
3	AGGGAAGGGA	147	IGHV4-61_08	IGHJ3_02	0,47	n/a	N	48,54
4	AGGGAAGGCC	225	IGHV2-70_11	IGHJ4_02	0,46	Y	Y	100,00
5	AGGCAAGGGG	276	IGHV3-33_05	IGHJ6_02	0,36	Y	Y	100,00
6	AGGGAAGGGA	222	IGHV3-7_01	IGHJ4_02	0,12	Y	Y	100,00

B

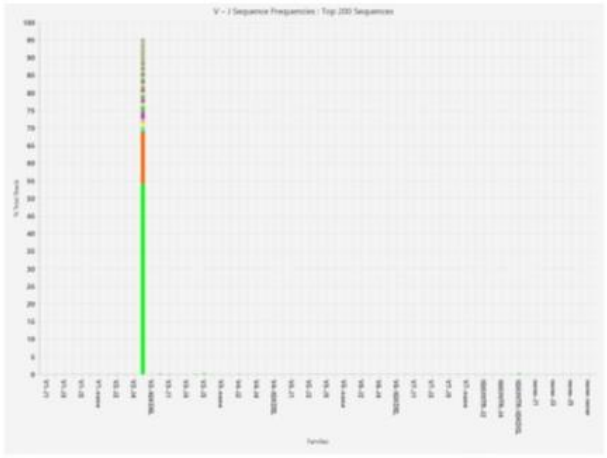

Rank	Sequence	Length	V-gene	J-gene	%total reads	V-coverage
1	AAAGTCTCC	140	IGKV2D-30 01	IGKJ5 01	95.65	4126
2	AAAGTCTCC	140	IGKV2D-30_01	IGKJ5_01	0.34	4126
3	AAAGTCTCC	130	IGKV2D-30 01	IGKJ5 01	0.33	26.91
4	AAAGTCACC	140	IGKV2D-30_01	IGKJ5_01	0.26	26.91
5	AACAGGGCC	149	IGKV3-11_01	IGKJ5_01	0.25	97.71
6	AGAGCCGCG	238	IGKINTR	IGKDEL	0.23	100.00
7	AAAGTCTCT	140	IGKV2D-30_01	IGKJ5_01	0.17	26.91
8	AGCAGGGCC	150	IGKV3D-20 01	IGKJ4 01	0.12	94.66
9	AAAGTCTCC	140	IGKV2D-30_01	IGKJ5_01	0.1	4126
10	AGCAGGGCC	149	IGKV3D-20 01	IGKJ1 01	0.06	99.24

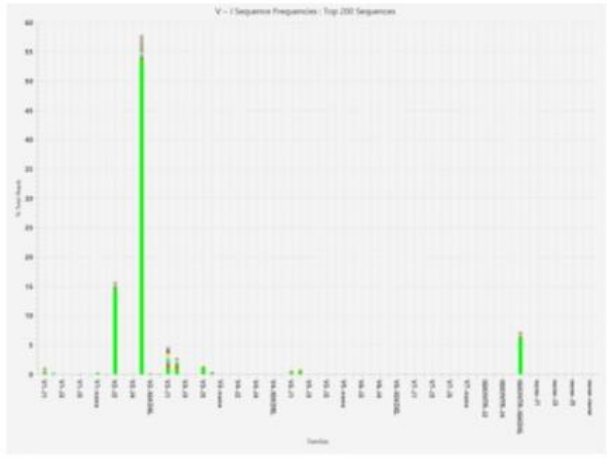

Rank	Sequence	Length	V-gene	J-gene	%total reads	V-coverage
1	AAAGTCTCC	140	IGKV2D-30 01	IGKJ5 01	58.64	4126
2	AAAGCCTCG	245	IGKV2-30_01	IGKJ2_02	16.47	100.00
3	AGAGCCGCG	238	IGKINTR	IGKDEL	6.14	100.00
4	AGCAGGGCC	151	IGKV3D-20_01	IGKJ5_01	1.33	99.24
5	AGCAGGGCC	152	IGKV3D-20_01	IGKJ1 01	1.22	98.47
6	AACAGGGCC	155	IGKV3-11 01	IGKJ2 01	1.09	100.00
7	AGCAGGGCC	148	IGKV3D-20_01	IGKJ1_01	0.96	97.71
8	AACAGGGCC	148	IGKV3-11 01	IGKJ1 01	0.9	96.95
9	AACAGGGCC	149	IGKV3-11_01	IGKJ2_02	0.79	100.00
10	ACCAGGGCC	133	IGKV3D-7 01	IGKJ1 01	0.76	85.5

***Figure 10. A**, Example of a case showing the same IGH clonality in both compartments, lymph node (**left panel**) and plasmatic ctDNA (**right panel**). The percentage of total reads is shown on the y-axis, and each V-J rearrangement is represented along the x-axis. Each color within the bars of the histogram represents a unique DNA sequence. **Bottom panels**: sequence corresponding to the tumor-specific clone is highlighted in yellow. **B**, Example of a case showing the same IGK clonality in both compartments, lymph node (**left panel**) and plasmatic ctDNA (**right panel**). The percentage of total reads is shown on the y-axis, and each V-J rearrangement is represented along the x-axis. Each color within the bars of the histogram represents a unique DNA sequence. **Bottom panels**: sequence corresponding to the tumor-specific clone is highlighted in yellow.*

Also, clonotype frequencies were compared between the two compartments analyzed at diagnosis. Clonotype frequencies were calculated as the number of sequencing reads for each clonotype divided by the total number of passed sequencing reads in the sample. The median clonotype frequency found in lymph nodes was 70.23% (range, 2.96–98.97), while in the plasma was 58.61% (range, 2.34–99.36). In cases where a different clonality was detected on ctDNA, the median frequency on lymph nodes was 50.68% (range, 2.5–97.12).

Among cases with no clonality detected on ctDNA, the median frequency on lymph nodes was 20.99% (range, 4.44–96.05). There was a trend, but not statistically significant, between the clonotypic frequency in the lymph node and the probability of identifying the same clonotype in the ctDNA.

Interestingly, a greater clonal heterogeneity was identified at baseline in the plasma than in the lymph node. Overall, on tumor biopsies the heterogeneity rate was of 24.2%, while on ctDNA a heterogeneity of 75.8% was identified (Figure 11).

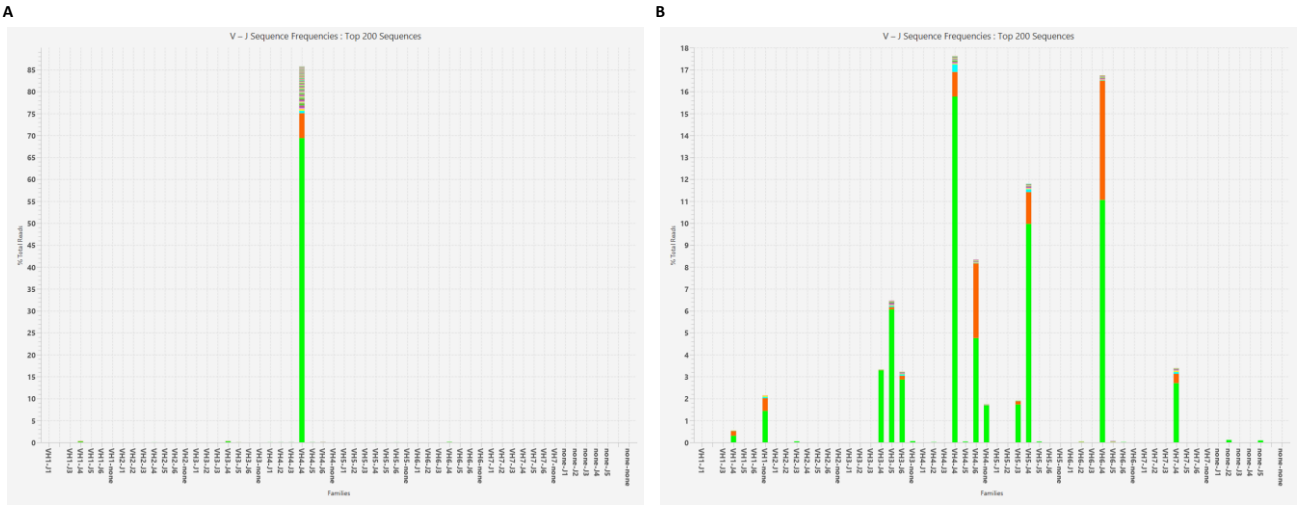

Figure 11. *Example of case with heterogeneity between the two compartments. (**A**) Lymph node, (**B**) plasmatic ctDNA.*

4. CORRELATION OF BASELINE CLONOTYPE WITH VARIOUS CLINICAL VARIABLES

The clonotype detection on paired samples (lymph node and baseline ctDNA) and the respective clonal frequencies were correlated with pre-treatment clinical characteristics including histology, stage, LDH elevation, IPI, B symptoms, extra nodal disease, and PS (Table 4) (for the clonotype frequency cut-off of 50%, see below).

***Table 4**. Correlations of the clonotype frequency on lymph node with pre-treatment clinical characteristics.*

		Clonotype frequency on lymph node						
		<50%		≥50%		Total		
		N	%	N	%	N	%	p value
Diagnosis	DLBCL	6	100.0%	15	88.3%	21	91.3%	0.54
	FL 3B	0	0.0%	2	11.8%	2	8.7%	
IPI	0	2	12.5%	5	16.7%	7	15.2%	0.35
	1.00	5	31.3%	6	20.0%	11	23.9%	
	2.00	5	31.3%	5	16.7%	10	21.7%	
	3.00	3	18.8%	5	16.7%	8	17.4%	
	4.00	1	6.3%	9	30.0%	10	21.7%	
PS	0	6	100.0%	11	64.7%	17	73.9%	0.23
	1	0	0.0%	4	23.5%	4	17.4%	
	2	0	0.0%	2	11.8%	2	8.7%	
LDH elevated	No	8	50.0%	17	56.7%	25	54.3%	0.66
	Yes	8	50.0%	13	43.3%	21	45.7%	
Stage	I	3	18.8%	4	13.3%	7	15.2%	0.8
	II	3	18.8%	9	30.0%	12	26.1%	
	III	5	31.3%	7	23.3%	12	26.1%	
	IV	5	31.3%	10	33.3%	15	32.6%	
B-Symptoms	No	10	90.9%	18	72.0%	28	77.8%	0.2
	Yes	1	9.1%	7	28.0%	8	22.2%	
Extra nodal disease	No	6	75.0%	7	30.4%	13	41.9%	0.03
	Yes	2	25.0%	16	69.6%	18	58.1%	

No statistically significant differences were found between the clonotype frequencies on both lymph node and baseline ctDNA and histology, LDH levels, IPI and B symptoms.

Contrariwise, there was a trend in the association of ctDNA clonotype detection with disease stage (Chi-square test; p=0.122). Among cases with a clone successfully identified on ctDNA, 57.9% were stage I-II and 81.5% were stage III-IV. Of the cases with no identified clone, 21.1% were stage I-II and only 3.7% were stage III-IV.

There was a moderate correlation between the clonotype frequencies on the lymph node and the extra nodal disease (ANOVA; p=0.03); a correlation trend, but not significantly different, was found between ctDNA clonal frequencies and the extra nodal disease (p=0.074).

A ROC curve was created to identify the clonotype frequency threshold that at diagnosis could best predict the PFS. Only on the lymph node a good correlation was found, identifying a frequency cut-off of 50%. Using this threshold, patients with values higher than 50% had significantly inferior rates of PFS than those with lower values (p=0.05; Figure 12). The run parameters were all comparable across the different experiments (Table 5), fulfilling the criteria of clonality definition reported in the Methods section.

Table 5. *Run parameters showing the percentages of Q30 and the number of sequencing reads per FFPE samples.*

No	% Total Reads	Total Read Count	IndexQ30
ID29	95.65	52038	97.69
ID2	94.22	658543	96.45
ID14	97.77	1327600	93.08
ID17	58.75	128517	94.25
ID19	49.97	185750	95.14
ID21	68.68	283783	91.87
ID22	50.97	589432	96.05
ID57	20.32	105460	95.54
ID53	71.61	16310	92.41
ID67	45.56	1178809	95.66
ID68	46.96	253741	94.07
ID79	2.96	376064	92.29
ID72	98.97	504501	94.95
ID78	74.85	65730	95.32
ID85	59.67	379745	91.88
ID86	13.30	763455	95.79
ID3	23.31	95210	94.99
ID6	2.50	67017	94.19
ID34	4.66	588932	95.64
ID81	96.05	556724	95.27
ID83	73.58	458972	94.07
ID84	40.78	10633	88.57
ID87	97.12	552493	94.67
ID015	78.95	21507	94.34
ID028	91.44	613118	92.53
ID002	19.33	49464	94.89
ID012	90.46	1241056	93.83
ID009	83.00	44870	90.27
ID008	60.42	702450	93.46
ID007	97.14	1241176	88.74
ID027	89.54	366729	90.06
ID025	60.58	1083450	94.62
ID003	7.71	827625	93.8
ID023	70.92	564281	94.68
ID039	96.53	448626	94.17
ID004	70.23	1604541	96.38
ID010	20.25	40477	90.97
ID030	67.43	80295	93.78
ID021	90.74	887135	93.11
ID026	47.77	64021	93.58
ID031	20.99	743127	94.58
ID016	86.53	474281	91.91
ID032	70.72	284859	95.91
ID013	4.44	546316	93.32
ID042	89.00	45530	93.03
ID043	85.60	87798	92.44

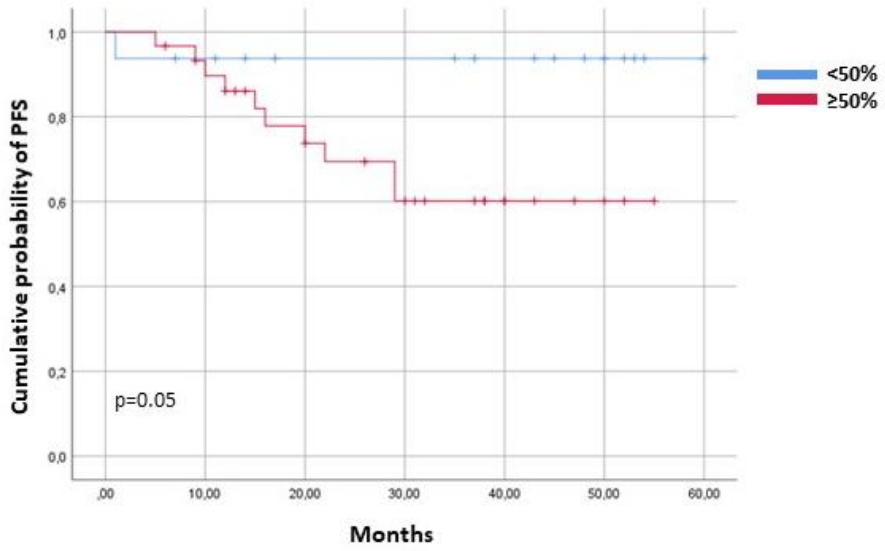

Figure 12. *Kaplan-Meier estimates of PFS in patients stratified by lymph node clonotype frequencies at diagnosis.*

Statistically significant differences were found when correlating the lymph node clonotype frequencies with the PS. All patients with a clonotype frequency less than 50% had a PS=0, and no events have been reported. Among patients with a clonotype frequency ≥50%, 11 had a PS=0 and 2 relapses were reported, 4 had a PS=1 with 3 relapses reported, and 2 had a PS=2 with 2 relapses (Figure 13).

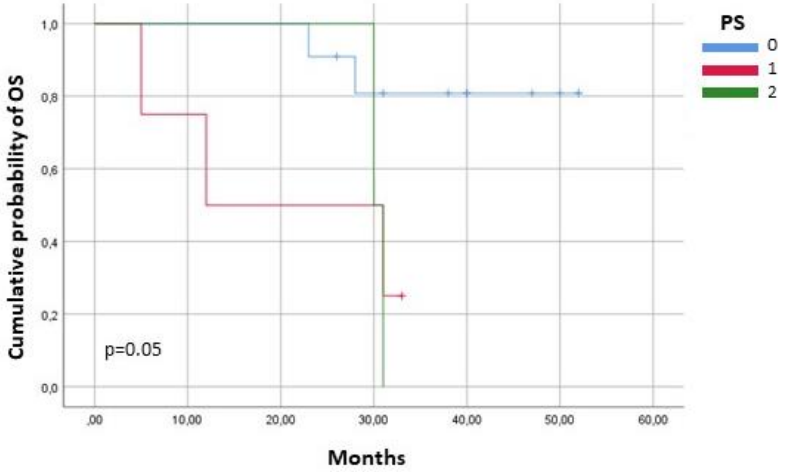

CF (%)	PS	Total	R/R	Disease-free
<50	0	6	0	6
≥50	0	11	2	9
	1	4	3	1
	2	2	2	0
Total	Total	23	7	16

Figure 13. *Kaplan-Meier estimates of OS in patients stratified by PS.*
PS, Performance Status; CF, Clonotype Frequency; R/R, Relapsed/Refractory.

Finally, the identification of a clonal marker on the lymph node *per sè* was not found indicative of prognosis (Figure 14). The same result was found on baseline ctDNA (data not shown).

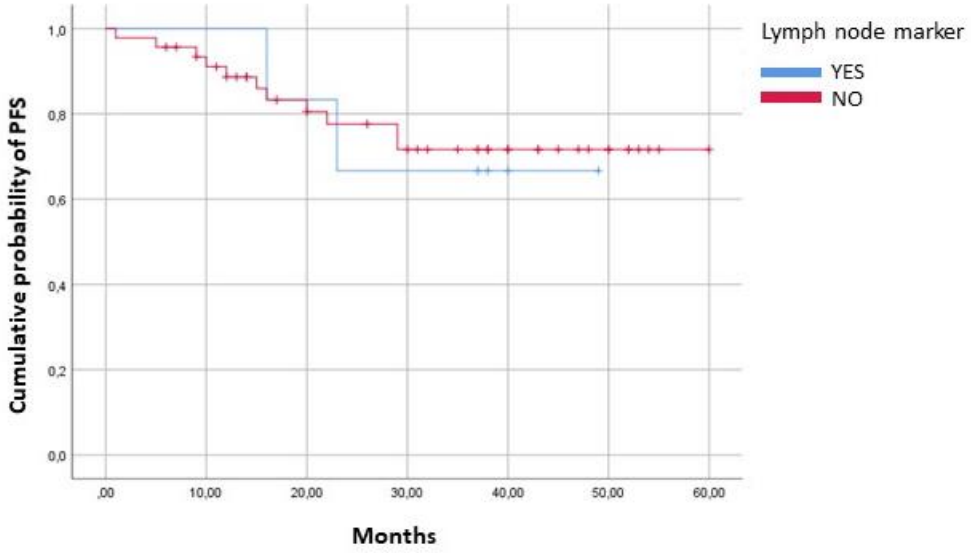

Figure 14. *PFS in patients stratified by lymph node marker identification*

5. LONGITUDINAL MONITORING OF ctDNA LEVELS

Longitudinal analysis of the plasmatic ctDNA samples was assessed during chemotherapy, at the end of treatment, and at relapse/progression in 26 patients (17 from Rome and 9 from Novara), selected among those with a concordance in clonality in the lymph node and plasma compartments analyzed at diagnosis. A total of 77 longitudinal plasma samples were studied: 33.8% at interim, 20.8% at the end of treatment, 19.5% at month +6, 15.6% at month +12, and 10.4% at month +24.

The mean plasma cfDNA concentration from all the longitudinal samples was 32.06 ng/mL (range, 3.94–110.4).

INTERIM EVALUATION

Upon treatment, ctDNA evaluation was possible in 26 patients: in 18 the basal tumor clonotype disappeared, in 6 persisted and in 2 a clonal shift was observed (for the latter cases with a clonal shift, see paragraph 6). At the interim CT, 10 patients showed a complete response, 15 a partial response and 1 a stable disease.

Nine/26 patients (34.6%) subsequently experienced disease progression and in 6 of 9 patients the basal ctDNA clonotype did not disappear during treatment. All patients were in partial response/stable disease according to CT ad interim.

Conversely, for 17/26 patients (65.4%) belonging to the non-progressive group, the ctDNA clonotype disappeared from the plasma at interim in 15/17 cases. At the interim CT, 6/15 showed a partial response and 9/15 a complete response by CT.

Overall, among the 8 patients with detectable interim ctDNA, 6 (75%) clinically progressed, after 5-29 months from diagnosis. One patient showed refractory disease. By contrast, only 3 (16.7%) of 18 patients with undetectable interim ctDNA clinically progressed after 16-29 months from diagnosis, none with early progression.

Thus, at interim MRD negativity on ctDNA was predictive for prognosis and identified patients with long-term disease control, as shown in Figure 15 A.

Overall, the concordance between molecular disease detected by ctDNA and radiological disease detected by interim CT was 69.2%. Among the discordances, only two patients showed undetectable ctDNA and a partial response and subsequently relapsed, with a time to progression of 14 and 21 months, respectively.

Interestingly, interim ctDNA could stratify the prognosis of the 16 patients that showed a partial response at the interim CT, as shown in Figure 15 B.

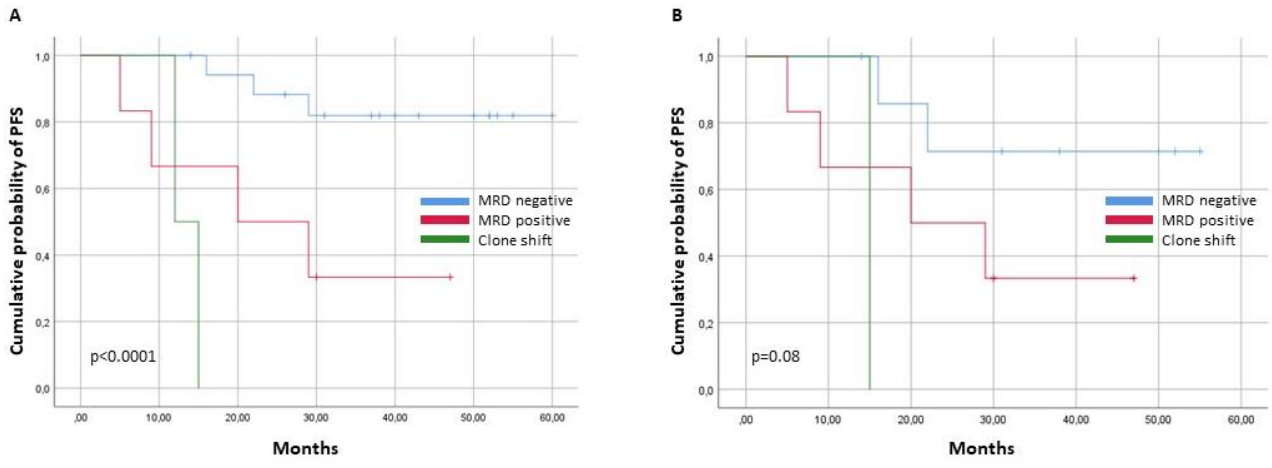

MRD interim	Total	R/R	Disease-free
Negative	18	3	15
Positive	6	4	2
Clone shift	2	2	0
Total	26	9	17

Interim response	MRD interim	Total	R/R	Disease-free
CR	Negative	10	1	9
PR	Negative	8	2	6
	Positive	6	4	2
	Clone shift	1	1	0
SD/PD	Clone shift	1	1	0
Total	Total	26	9	17

Figure 15. *Kaplan-Meier estimates of PFS according to ctDNA interim-MRD status in all patients (**A**), and in patients in PR at the interim CT scan (**B**).*
CR, complete response; PR, partial response; SD/PD, stable disease/progressive disease.

DISEASE MONITORING AT THE END OF TREATMENT AND DURING SURVEILLANCE

Fifty-one plasma samples from 16 patients were available at the end of therapy and during surveillance, of which 7 patients (43.7%) eventually relapsed.

By the end of treatment, 85.7% (6 of 7) of relapsed patients had a complete response according to PET/CT, even though molecular disease was detected on ctDNA. One relapsing patient (#ID023)

showed a stable disease by PET/CT after therapy and had detectable disease on ctDNA. Overall, the median time from the end of therapy evaluation and the time of relapse was 11.5 months (range, 3–24 months).

Among these 7 patients, slightly different kinetics of ctDNA have been observed. The most frequent pattern was no clearance of molecular disease until the clinical progression (6 out of 7, 85.7%). In one patient (#ID009), a transient clearance (at month+6/month+12) was registered followed by positivity of ctDNA MRD at progression. Patients who never cleared ctDNA had a median time to progression of 16.5 months, compared with 21 months for patient #ID009.

At the time of relapse/progression, all patients with plasma sample available (5 of 5, 100%) had detectable disease on ctDNA.

Five of the 7 relapsed patients (71.4%) died of disease progression. The median survival after recurrence was of 11 months (range, 2–19).

Nine of the 16 patients (56%) longitudinally monitored had a rapid clearance of ctDNA from plasma and remained negative for all the subsequent follow-ups. Two out of 9 patients had absence of metabolic response according to PET/CT, and the remaining patients had a complete response. None of the 9 patients experienced relapse. The median survival for this group of patients was 46 months (range, 26–53 months). Figure 16 shows the ctDNA results of all patients longitudinally monitored.

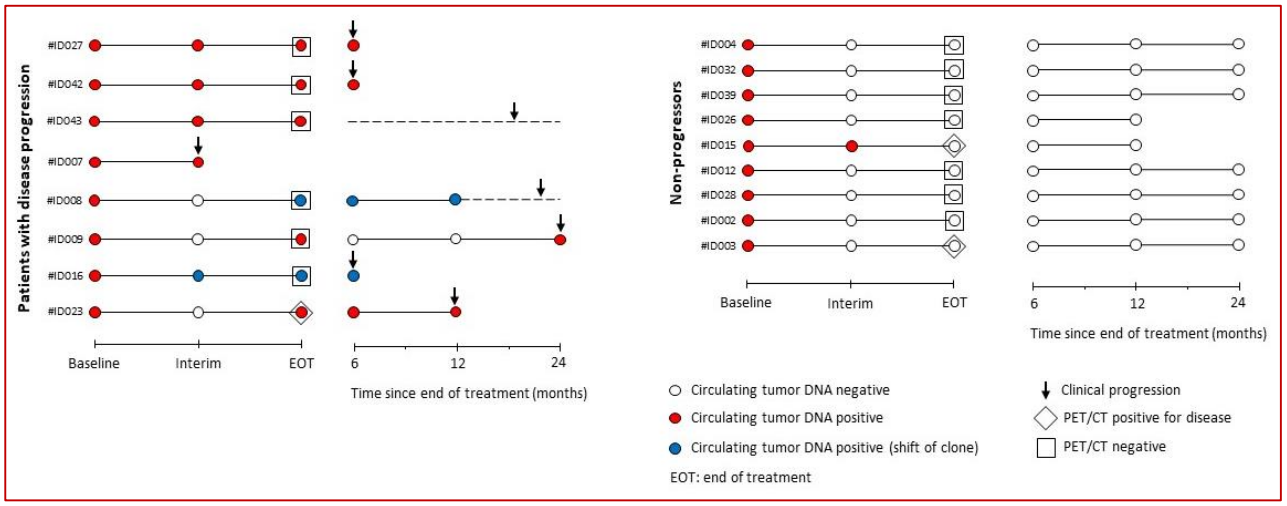

Figure 16*. Molecular disease evaluation on ctDNA for all patients who completed treatment and either did not progress or had progression within 24 months after treatment.*

Overall, plasma ctDNA evaluation had no false positives at the end of treatment, yielding a specificity of 100%. PET/CT scans from the same patients showed a concordance with ctDNA analysis of 50%. The prognostic role of molecular response was further analyzed within patients with a complete response according to the end of therapy PET/CT. DLBCL patients with undetectable *IG* on ctDNA at the end of therapy show a superior PFS compared with patients with positive ctDNA. Indeed, all

relapsed patients had detectable molecular disease at the end of treatment, while none of the patients with negative ctDNA ultimately relapsed (Figure 17).

A Chi-square test was used to correlate the lymph node clonotype frequencies and the ctDNA positivity at the end of treatment. All patients with a clonal frequency lower than 50% were ctDNA negative, while patients with a clonal frequency ≥50% all had presence of disease in the plasma at the end of treatment (Figure 18). Therefore, a lower or higher representation of the clonal marker on the lymph node could be indicative of the MRD status by the end of therapy.

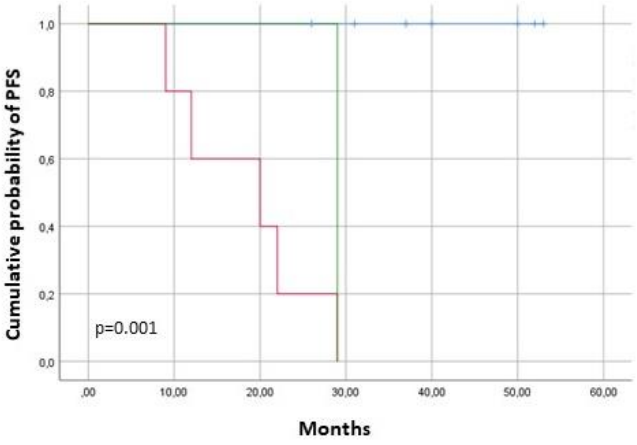

EOT response	MRD EOT	Total	R/R	Disease-free
CR	Negative	7	0	7
	Positive	5	5	0
	Clone shift	1	1	0
PR/SD	Negative	2	0	2
	Positive	1	1	0
Total	Total	16	7	9

Figure 17. *Kaplan-Meier estimates of PFS for patients in CR at the end of therapy, stratified accordingly to the MRD status.*

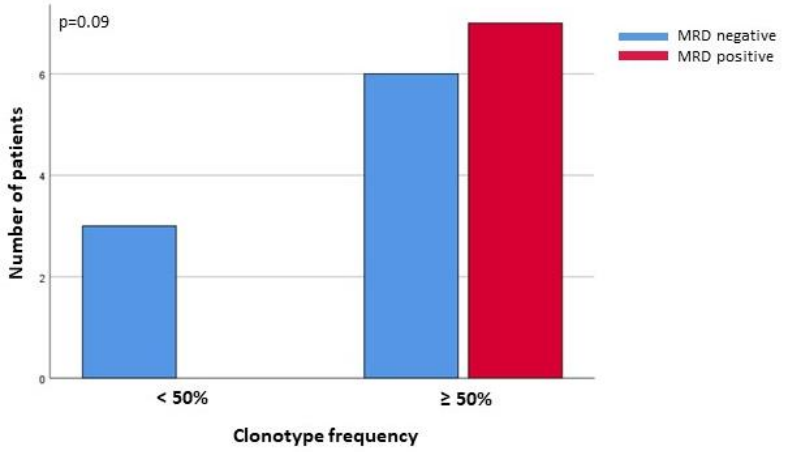

Figure 18. *Chi-square test comparing lymph node clonotype frequencies and MRD status at the EOT.*

6. CLONAL EVOLUTION

One advantage of the NGS technology is that all the *IG* genes rearrangements are simultaneously captured, enabling to comprehensive characterize the genetic diversity and to follow clonal selection. In several hematologic malignancies the clinical relapse is often caused by the rise of a more

aggressive subclone after treatment, which was mostly present, but not predominant, at the initial diagnosis.

In this study, the paired diagnostic and relapse plasma samples of all but two patients harbored the same clonal rearrangement. In two patients (#ID016 and #ID008), a different clonality was observed between the plasma sample of the recurrence and that of the diagnosis. Moreover, the different clone was not present in the FFPE specimen and was still an *IGH* rearrangement in both cases (Figure 19).

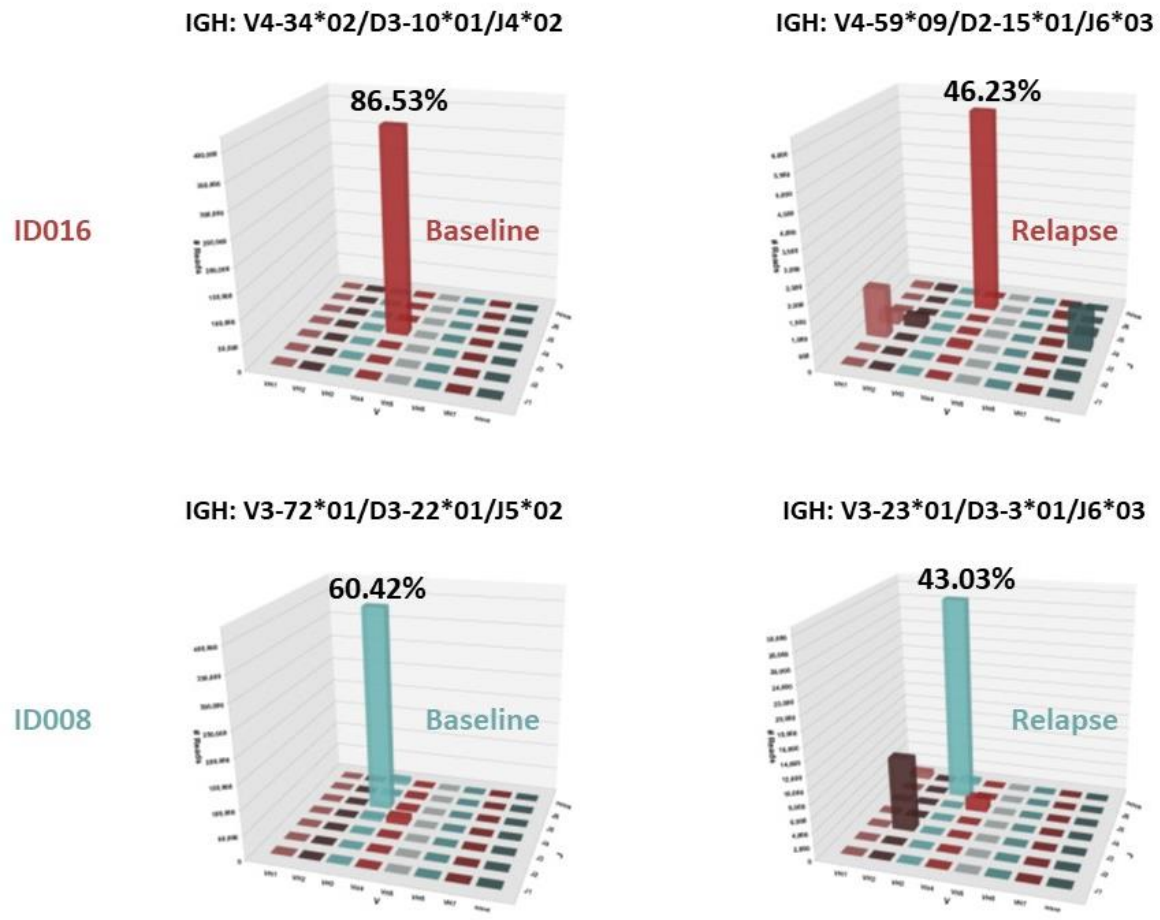

Figure 19. *Comparison of the baseline clone identified in the FFPE sample and the clone identified in the ctDNA at relapse. The respective IGH rearrangements and clonal frequencies are reported.*

An early-divergent modality of clonal evolution was observed. The clonality detected at relapse was already previously present on ctDNA at an earlier phase; for case #ID016 starting from the evaluation at interim and for case #ID008 from the end of treatment (Figure 20). This evidence supports the idea that the relapse-related clonotypes were selected early during treatment for an intrinsic resistance, being likely responsible of the progression.

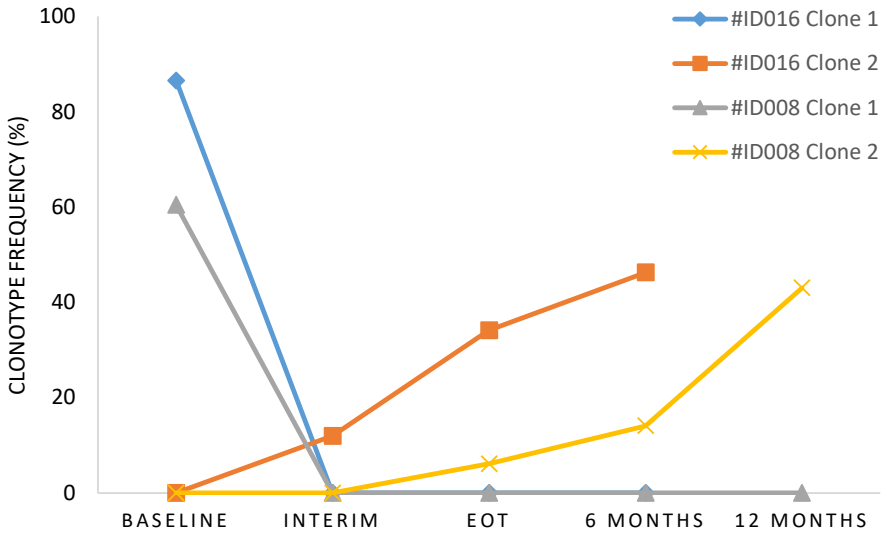

Figure 20. *Clonal evolution in two relapsed patients. In both cases the tumor clonotype detected in the two compartments (lymph node biopsy and plasmatic ctDNA) was not detected in the subsequent evaluations. A different clonotype emerged at the interim time point (for case #ID016) and at the end of treatment (for case #ID008) that was not present at baseline in either compartment.*

CONCLUSIONS

First-line combination chemotherapy cures ~60% of DLBCL cases, and the disease that relapses or is refractory to first-line therapy is difficult to rescue (Crump *et al*, 2017). Approximately 10 to 15% of patients treated with R-CHOP have primary refractory disease (i.e., an incomplete response or a relapse within 6 months after treatment), and an additional 20 to 25% will have a relapse after an initial response, typically within the first 2 years of the initial diagnosis. (Maurer *et al*, 2014). In line with what was reported, in the cohort analyzed for this study all the relapses (21% of 52 cases) occurred within 24 months from the end of treatment.

Complete eradication of disease is required to cure DLBCL, yet the current response criteria do not incorporate markers that detect the presence of subclinical molecular disease at the end of therapy, the so called MRD, that has become the standard in other hematologic diseases (Bassan *et al*, 2019; Berry *et al*, 2017; Hallek *et al*, 2018; Landgren *et al*, 2019). The current standard for monitoring DLBCL response to therapy is PET/CT scan or other imaging techniques (Tilly *et al*, 2015), with associated radiation risks and a limit of detection that may miss residual disease. Up to ~15% of DLBCL will ultimately relapse despite achieving a PET/CT negative complete response, and a proportion of patients with positive scans will never progress (Adams *et al*, 2015).

Indeed, whenever a patient achieves a complete clinical remission, a number of different scenarios may actually take place, including the full eradication of the neoplastic clone or the persistence of residual tumor cells capable of giving rise to a full clinical relapse within months or years.

The best classification of patients with good versus poor prognosis is reached by the end of treatment PET/CT. However, this timepoint would be rather late to adapt treatment strategies according to the quality and depth of response. Interim PET/CT performed after two cycles of treatment has been tested for the early identification of chemorefractory patients, as they are candidates for treatment intensification to maximize the chances of cure, as well as to early identify good-risk patients, as they are candidates for treatment de-escalation to avoid both short- and long-term complications of chemoradiotherapy (Moghbel *et al*, 2017). As reported, the positive predictive value of interim PET/CT in DLBCL is 50%, and the negative predictive value of interim PET/CT is 70% (Mamot *et al*, 2015). This means that 30% of DLBCL patients are misclassified by interim PET/CT as R-CHOP sensitive but will ultimately relapse.

Promising results from the present study show that the analysis of molecular disease through ctDNA detection of *IG* rearrangements could overcome many of these limitations.

There is an increasing literature on ctDNA analysis in Hodgkin's and NHL, but the best developed area of interest is in DLBCL. Indeed, ctDNA in DLBCL was proven useful for diagnostic and prognostic purposes and has been explored also as a response-defining tool after treatment.

In terms of diagnosis and prognosis, ctDNA can provide a landscape of DLBCL-associated mutations (Rossi *et al*, 2017), that has prognostic implication, particularly useful at disease onset when the diagnostic lymph node biopsy is not sufficient or adequate and difficult to be repeated for a molecular stratification. Moreover, the levels of ctDNA before treatment can be used as a measure of tumor burden with prognostic implications.

In terms of the assessment of response to therapy and relapse monitoring, ctDNA can be a non-invasive tool to monitor MRD in DLBCL, a disease in which lymphoma cells do not circulate in the PB or BM, therefore the type of MRD monitoring used in other NHL or leukemias on genomic DNA is not applicable. Several studies tried to monitor MRD in DLBCL through a targeted-gene mutations monitoring or/and an *IG*-NGS monitoring (see below), both proving informative on patients' outcome (Table 6 and 7 and Introduction paragraph 6 and 7).

Table 6. *Studies demonstrating the value of ctDNA-based response assessment during treatment. Adapted from Lauer et al, 2022.*

	Author	PMID/doi	Parameter	Method	No. of patients	Prediction of PFS / EFS	Prediction of OS
DLBCL	Roschewski et al.	25842160	ctDNA det. vs. undet. after c2	IgHTS	108	TTP $p < 0.0001$	*n.s.*
	Kurtz et al.	30125215	2-log drop of ctDNA at c2d1	Panel-directed NGS[a]	Validation set 1:73	$p = 0.015$	$p < 0.001$
			2.5-log drop of ctDNA at c3d1			$p < 0.001$	$p = 0.0047$
	Kurtz et al.	34294911	ctDNA det. vs. undet. at c3d1[b]	Panel-directed NGS[c]	52	$p = 0.0047$	NA
	Merryman et al.	10.1182/blood-2020-140965	ctDNA det. vs. undet. in ASC sample	IgHTS	97	$p < 0.001$	$p = 0.037$
	Frank et al.	34133196	ctDNA det. vs. undet. at d21 after CAR T-cell therapy[d]	IgHTS	57	$p < 0.0001$	$p = 0.0012$
	Assouline et al.	27166360	ctDNA increase vs. decrease at d15	Panel-directed NGS, ddPCR	25	$p = 0.0049$	$p = 0.00117$
	Meriranta et al.	34932792	ctDNA det. vs. undet. after 3 cycles	Panel-directed NGS	58	*n.s.*	*n.s.*

Table 7. *Studies demonstrating the prognostic value of ctDNA after therapy and during surveillance. Adapted from Lauer et al, 2022.*

	Author	PMID/doi	Parameter	Method	No. of patients	Prediction of PFS / EFS	Prediction of OS	Other findings
DLBCL	Roschewski et al.	25842160	Relapse detection by ctDNA during surveillance	IgHTS	107	NA	NA	ctDNA detection in 88% of relapses, median lead time of 3.5 months
	Scherer et al.	27831904	ctDNA det. vs. undet. during surveillance	Panel-directed NGS[a]	25	$p = 0.0003$	*n.s.*	ctDNA detection in 100% of relapses, mean lead time of 2 months
	Kumar et al.	10.1182/blood-2020-138889	Relapse detection by ctDNA during surveillance	IgHTS	43	NA	NA	ctDNA detection in 56% of relapses
	Merryman et al.	10.1182/blood-2020-140965	ctDNA detection post ASCT	IgHTS	20[b]	NA	NA	ctDNA detection in 90% of relapses
	Frank et al.	34133196	Relapse detection by ctDNA after CAR T-cell therapy	IgHTS	30	NA	NA	ctDNA detection in 94% of relapses
	Kurtz et al.	34294911	ctDNA det. vs. undet. end of treatment	Panel-directed NGS[c]	19	$p = 2.7 \times 10^{-6}$	NA	NA
	Meriranta et al.	34932792	ctDNA det. vs. undet. end of treatment	Panel-directed NGS	71	$p = 0.00098$	$p = 0.0049$	NA

In this thesis, an NGS-based assay for IG rearrangements was tested to prove its suitability for clonotype identification and MRD analysis in plasma samples of newly diagnosed DLBCL patients. NGS-based *IG* rearrangement assays have been successfully used in the clonal characterization and subsequent disease monitoring in various B-cell lineage malignancies, offering the proof-of-principle

that NGS is more specific and potentially more sensitive than conventional low-throughput technology.

Based on the current study, NGS based *IG*-clonality analysis is a robust method for the initial clonal characterization in patients with DLBCL. Indeed, clonal *IG* gene rearrangements were identified as disease biomarkers in 88.5% (46 of 52) of analyzed samples, in line with what was previously published by Kurtz *et al* (2015). Moreover, the incorporation of primer sets targeting all the framework regions of *IGH* (FR1, FR2, and FR3), as well as *IGK*, has increased the successful rate of identification of tumor-related clones. A potential reduced applicability of this approach has been reported in some DLBCL of the germinal center type because of SHM, leading to difficulties in identifying clonotypic sequences (Kurtz *et al*, 2015).

Among the 46 patients with an established tumor clonotype, pre-treatment ctDNA clonality was detected in plasma in 41 (89%). Identical clonality calls between paired samples were found in 33/41 cases, giving an informativity rate of 80.5%; therefore, plasma from PB could likely be an informative and non-invasive source of DNA for studying DLBCL patients at diagnosis. Moreover, by comparing tumor biopsies with ctDNA, a higher degree of clonal heterogeneity was found on ctDNA, which could support its role in recapitulating the molecular heterogeneity across the different disease sites.

For MRD monitoring, assays based on plasma samples can be affected by the low concentrations of extracted cfDNA, which in turn, limits the maximum amount of DNA that can be used in each reaction and so the assay sensitivity. Indeed, preanalytical and analytical factors can have different impact on cfDNA applicability and some efforts have been made to validate a protocol to overcome these biases (Soscia *et al*, 2023). However, in this thesis the NGS assay proved to be highly sensitive giving reliable results also in this setting of critical material.

At the interim time point during treatment, different studies showed how quantification of ctDNA coupled with PET/CT could improve the accuracy of residual disease assessment compared to the sole PET/CT. Indeed, patients inconsistently judged as interim PET/CT positive, but having a negative liquid biopsy, are actually cured, while patients inconsistently judged as interim PET/CT negative, but with a positive liquid biopsy, are actually not cured (Spina *et al*, 2018; Kurtz *et al*, 2018). These results generated the hypothesis that ctDNA may complement interim PET/CT in informing on DLBCL patients' outcome. In line with these observations, the findings reported in this thesis show the capacity of ctDNA to effectively monitor disease status at the molecular level in patients with DLBCL. Molecular disease detected on ctDNA at interim was significantly associated with subsequent relapses. It was positive in 6 of 9 (66.7%) and in 2 of 17 (11.8%) patients belonging to the relapsed and non-relapsed group, respectively. According to CT scans, 8 of 9 (88.9%) relapsed patients had a partial response or a stable disease, and 8 of 17 (47.1%) non-relapsed patients had

imaging scans positive for the disease. Overall, patients with negative interim ctDNA had excellent outcomes: 3 events were reported in 18 ctDNA negative patients, and 6 events in 8 ctDNA positive patients ($p<0.0001$). Interestingly, ctDNA evaluation could allow to better categorize the partial response by interim CT scans, as 8 patients with a partial response were ctDNA negative and two relapsed (25%), and 7 patients were ctDNA positive and 5 relapsed (71.4%).

At the end of treatment, ctDNA proved a promising biomarker for the identification of patients at high risk of relapse, as the best PFS was observed in patients who achieved MRD negativity at this time point. Indeed, 100% (7 of 7) of patients who subsequently relapsed were positive on ctDNA. Of these 7 patients, only one had a PET/CT positive result at the end of treatment. Moreover, 9 patients were negative on ctDNA and never experienced relapse; 2/9 (22.2%) showed a false-positive result by PET/CT.

After therapy, surveillance monitoring with PET/CT scans for DLBCL has proven neither effective for improving clinical outcomes nor cost-effective when applied to all patients in first remission (Thompson *et al*, 2014; Huntington *et al*, 2015). On the contrary, surveillance ctDNA monitoring of tumor-related clones identified risk of recurrence before clinical evidence of disease in most patients. Among patients in remission, mostly had undetectable MRD in ctDNA: of 77 plasma samples longitudinally tested, we noted only 3 (3.9%) discordantly positive samples in patients with no progression.

In patients who relapsed early (within 6 months after treatment), interim ctDNA predicted the relapse in all cases. In patients who relapsed after the assessment at month +6, ctDNA was informative of relapse, at the evaluation time point before the relapse, in all but one patient.

Therefore, ctDNA evaluation both at interim, at the end of treatment and thereafter allows to better stratify DLBCL patients' outcome.

These results highlight the emerging concept that testing ctDNA is a non-invasive and dynamic method that can be used as often as necessary to detect subclinical disease, as the longitudinally monitoring of tumor-related clones should theoretically lead to 100% specificity.

In addition to these results, serial monitoring of ctDNA after therapy for DLBCL may also inform on acquired resistance and clonal evolution. Undoubtedly, a notable advantage of *IG*-NGS testing is the ability to broaden the molecular assessment to encompass the entire immune repertoire, the clonal architecture and clonal dynamics over time. In this study, two patients exhibited different clonality between the plasma sample of the recurrence and that of the tumor biopsy; the divergent clone was already present in the circulation at an early stage. One limit of the *IG*-NGS based monitoring compared to the liquid biopsy approach is the lack of information on the mutational evolution of the

lymphoma, that could lead to the identification of biomarker of resistance and/or target for alternative therapies.

In conclusion, despite the reported positive results on ctDNA analysis in DLBCL patients, the current literature is mostly based on retrospective cohorts. Prospective studies are now needed to establish the feasibility of real-time ctDNA evaluation for diagnosis and follow-up, incorporating this tool into clinical trials to better characterize the clinical utility of these findings (Pirosa *et al*, 2022). Moreover, the broad application of this testing modality in routine practice is limited by the lack of standardized guidelines for validation and implementation processes.

The next future will determine how ctDNA can integrate with established imaging tools for a complementary monitoring of treatment response, and how ctDNA can be used as an earlier surrogate endpoint in risk-adapted clinical trials.

REFERENCES

1. Adams HJ, Nievelstein RA, Kwee TC. Prognostic value of complete remission status at end-of-treatment FDG-PET in R-CHOP-treated diffuse large B-cell lymphoma: systematic review and meta-analysis. Br J Haematol. 2015 Jul;170(2):185-91. doi: 10.1111/bjh.13420.

2. Alaggio R, Amador C, Anagnostopoulos I, Attygalle AD, Araujo IBO, Berti E, Bhagat G, Borges AM, Boyer D, Calaminici M, Chadburn A, Chan JKC, Cheuk W, Chng WJ, Choi JK, Chuang SS, Coupland SE, Czader M, Dave SS, de Jong D, Du MQ, Elenitoba-Johnson KS, Ferry J, Geyer J, Gratzinger D, Guitart J, Gujral S, Harris M, Harrison CJ, Hartmann S, Hochhaus A, Jansen PM, Karube K, Kempf W, Khoury J, Kimura H, Klapper W, Kovach AE, Kumar S, Lazar AJ, Lazzi S, Leoncini L, Leung N, Leventaki V, Li XQ, Lim MS, Liu WP, Louissaint A Jr, Marcogliese A, Medeiros LJ, Michal M, Miranda RN, Mitteldorf C, Montes-Moreno S, Morice W, Nardi V, Naresh KN, Natkunam Y, Ng SB, Oschlies I, Ott G, Parrens M, Pulitzer M, Rajkumar SV, Rawstron AC, Rech K, Rosenwald A, Said J, Sarkozy C, Sayed S, Saygin C, Schuh A, Sewell W, Siebert R, Sohani AR, Tooze R, Traverse-Glehen A, Vega F, Vergier B, Wechalekar AD, Wood B, Xerri L, Xiao W. The 5th edition of the World Health Organization Classification of Haematolymphoid Tumours: Lymphoid Neoplasms. Leukemia. 2022 Jul;36(7):1720-1748. doi: 10.1038/s41375-022-01620-2.

3. Alizadeh AA, Aranda V, Bardelli A, Blanpain C, Bock C, Borowski C, Caldas C, Califano A, Doherty M, Elsner M, Esteller M, Fitzgerald R, Korbel JO, Lichter P, Mason CE, Navin N, Pe'er D, Polyak K, Roberts CW, Siu L, Snyder A, Stower H, Swanton C, Verhaak RG, Zenklusen JC, Zuber J, Zucman-Rossi J. Toward understanding and exploiting tumor heterogeneity. Nat Med. 2015 Aug;21(8):846-53. doi: 10.1038/nm.3915.

4. Alizadeh AA, Eisen MB, Davis RE, Ma C, Lossos IS, Rosenwald A, Boldrick JC, Sabet H, Tran T, Yu X, Powell JI, Yang L, Marti GE, Moore T, Hudson J Jr, Lu L, Lewis DB, Tibshirani R, Sherlock G, Chan WC, Greiner TC, Weisenburger DD, Armitage JO, Warnke R, Levy R, Wilson W, Grever MR, Byrd JC, Botstein D, Brown PO, Staudt LM. Distinct types of diffuse large B-cell lymphoma identified by gene expression profiling. Nature. 2000 Feb 3;403(6769):503-11. doi: 10.1038/35000501.

5. Anderson T, Bender RA, Fisher RI, DeVita VT, Chabner BA, Berard CW, Norton L, Young RC. Combination chemotherapy in non-Hodgkin's lymphoma: results of long-term followup. Cancer Treat Rep. 1977 Sep;61(6):1057-66. PMID: 71205.

6. Armitage JO, Gascoyne RD, Lunning MA, Cavalli F. Non-Hodgkin lymphoma. Lancet. 2017 Jul 15;390(10091):298-310. doi: 10.1016/S0140-6736(16)32407-2.

7. Barrington SF, Mikhaeel NG, Kostakoglu L, Meignan M, Hutchings M, Müeller SP, Schwartz LH, Zucca E, Fisher RI, Trotman J, Hoekstra OS, Hicks RJ, O'Doherty MJ, Hustinx R, Biggi A, Cheson BD. Role of imaging in the staging and response assessment of lymphoma: consensus of the International Conference on Malignant Lymphomas Imaging Working Group. J Clin Oncol. 2014 Sep 20;32(27):3048-58. doi: 10.1200/JCO.2013.53.5229.

8. Bassan R, Brüggemann M, Radcliffe HS, Hartfield E, Kreuzbauer G, Wetten S. A systematic literature review and meta-analysis of minimal residual disease as a prognostic indicator in adult B-cell acute lymphoblastic leukemia. Haematologica. 2019 Oct;104(10):2028-2039. doi: 10.3324/haematol.2018.201053.

9. Basso K, Dalla-Favera R. Germinal centres and B cell lymphomagenesis. Nat Rev Immunol. 2015 Mar;15(3):172-84. doi: 10.1038/nri3814.

10. Berry DA, Zhou S, Higley H, Mukundan L, Fu S, Reaman GH, Wood BL, Kelloff GJ, Jessup JM, Radich JP. Association of Minimal Residual Disease With Clinical Outcome in Pediatric and Adult Acute Lymphoblastic Leukemia: A Meta-analysis. JAMA Oncol. 2017 Jul 13;3(7):e170580. doi: 10.1001/jamaoncol.2017.0580.

11. Cerhan JR, Kricker A, Paltiel O, Flowers CR, Wang SS, Monnereau A, Blair A, Dal Maso L, Kane EV, Nieters A, Foran JM, Miligi L, Clavel J, Bernstein L, Rothman N, Slager SL, Sampson JN, Morton LM, Skibola CF. Medical history, lifestyle, family history, and occupational risk factors for diffuse large B-cell lymphoma: the InterLymph Non-Hodgkin Lymphoma Subtypes Project. J Natl Cancer Inst Monogr. 2014 Aug;2014(48):15-25. doi: 10.1093/jncimonographs/lgu010.

12. Chapuy B, Stewart C, Dunford AJ, Kim J, Kamburov A, Redd RA, Lawrence MS, Roemer MGM, Li AJ, Ziepert M, Staiger AM, Wala JA, Ducar MD, Leshchiner I, Rheinbay E, Taylor-Weiner A, Coughlin CA, Hess JM, Pedamallu CS, Livitz D, Rosebrock D, Rosenberg M, Tracy AA, Horn H, van Hummelen P, Feldman AL, Link BK, Novak AJ, Cerhan JR, Habermann TM, Siebert R, Rosenwald A, Thorner AR, Meyerson ML, Golub TR, Beroukhim R, Wulf GG, Ott G, Rodig SJ, Monti S, Neuberg DS, Loeffler M, Pfreundschuh M, Trümper L, Getz G, Shipp MA. Molecular subtypes of diffuse large B cell lymphoma are associated with distinct pathogenic mechanisms and outcomes. Nat Med. 2018 May;24(5):679-690. doi: 10.1038/s41591-018-0016-8.

13. Cheson BD, Ansell S, Schwartz L, Gordon LI, Advani R, Jacene HA, Hoos A, Barrington SF, Armand P. Refinement of the Lugano Classification lymphoma response criteria in the era of immunomodulatory therapy. Blood. 2016 Nov 24;128(21):2489-2496. doi: 10.1182/blood-2016-05-718528.

14. Cheson BD, Fisher RI, Barrington SF, Cavalli F, Schwartz LH, Zucca E, Lister TA; Alliance, Australasian Leukaemia and Lymphoma Group; Eastern Cooperative Oncology Group; European Mantle Cell Lymphoma Consortium; Italian Lymphoma Foundation; European Organisation for Research; Treatment of Cancer/Dutch Hemato-Oncology Group; Grupo Español de Médula Ósea; German High-Grade Lymphoma Study Group; German Hodgkin's Study Group; Japanese Lymphorra Study Group; Lymphoma Study Association; NCIC Clinical Trials Group; Nordic Lymphoma Study Group; Southwest Oncology Group; United Kingdom National Cancer Research Institute. Recommendations for initial evaluation, staging, and response assessment of Hodgkin and non-Hodgkin lymphoma: the Lugano classification. J Clin Oncol. 2014 Sep 20;32(27):3059-68. doi: 10.1200/JCO.2013.54.8800.

15. Cirillo M, Craig AFM, Borchmann S, Kurtz DM. Liquid biopsy in lymphoma: Molecular methods and clinical applications. Cancer Treat Rev. 2020 Dec;91:102106. doi: 10.1016/j.ctrv.2020.102106.

16. Coiffier B, Thieblemont C, Van Den Neste E, Lepeu G, Plantier I, Castaigne S, Lefort S, Marit G, Macro M, Sebban C, Belhadj K, Bordessoule D, Fermé C, Tilly H. Long-term outcome of patients in the LNH-98.5 trial, the first randomized study comparing rituximab-CHOP to standard CHOP chemotherapy in DLBCL patients: a study by the Groupe d'Etudes des Lymphomes de l'Adulte. Blood. 2010 Sep 23;116(12):2040-5. doi: 10.1182/blood-2010-03-276246.

17. Crump M, Neelapu SS, Farooq U, Van Den Neste E, Kuruvilla J, Westin J, Link BK, Hay A, Cerhan JR, Zhu L, Boussetta S, Feng L, Maurer MJ, Navale L, Wiezorek J, Go WY, Gisselbrecht C. Outcomes in refractory diffuse large B-cell lymphoma: results from the international SCHOLAR-1 study. Blood. 2017 Oct 19;130(16):1800-1808. doi: 10.1182/blood-2017-03-769620.

18. Fisher RI, Gaynor ER, Dahlberg S, Oken MM, Grogan TM, Mize EM, Glick JH, Coltman CA Jr, Miller TP. Comparison of a standard regimen (CHOP) with three intensive chemotherapy regimens for advanced non-Hodgkin's lymphoma. N Engl J Med. 1993 Apr 8;328(14):1002-6. doi: 10.1056/NEJM199304083281404.

19. Frank MJ, Hossain NM, Bukhari A, Dean E, Spiegel JY, Claire GK, Kirsch I, Jacob AP, Mullins CD, Lee LW, Kong KA, Craig J, Mackall CL, Rapoport AP, Jain MD, Dahiya S, Locke FL, Miklos DB. Monitoring of Circulating Tumor DNA Improves Early Relapse Detection After Axicabtagene Ciloleucel Infusion in Large B-Cell Lymphoma: Results of a Prospective Multi-Institutional Trial. J Clin Oncol. 2021 Sep 20;39(27):3034-3043. doi: 10.1200/JCO.21.00377.

20. Friedberg JW. Relapsed/refractory diffuse large B-cell lymphoma. Hematology Am Soc Hematol Educ Program. 2011;2011:498-505. doi: 10.1182/asheducation-2011.1.498.

21. Gellert M. V(D)J recombination: RAG proteins, repair factors, and regulation. Annu Rev Biochem. 2002;71:101-32. doi: 10.1146/annurev.biochem.71.090501.150203.

22. Giné E, Sehn LH. Diffuse Large B-Cell Lymphoma: Should Limited-Stage Patients Be Treated Differently? Hematol Oncol Clin North Am. 2016 Dec;30(6):1179-1194. doi: 10.1016/j.hoc.2016.07.010.

23. Gisselbrecht C, Glass B, Mounier N, Singh Gill D, Linch DC, Trneny M, Bosly A, Ketterer N, Shpilberg O, Hagberg H, Ma D, Brière J, Moskowitz CH, Schmitz N. Salvage regimens with autologous transplantation for relapsed large B-cell lymphoma in the rituximab era. J Clin Oncol. 2010 Sep 20;28(27):4184-90. doi: 10.1200/JCO.2010.28.1618.

24. Hallek M, Cheson BD, Catovsky D, Caligaris-Cappio F, Dighiero G, Döhner H, Hillmen P, Keating M, Montserrat E, Chiorazzi N, Stilgenbauer S, Rai KR, Byrd JC, Eichhorst B, O'Brien S, Robak T, Seymour JF, Kipps TJ. iwCLL guidelines for diagnosis, indications for treatment, response assessment, and supportive management of CLL. Blood. 2018 Jun 21;131(25):2745-2760. doi: 10.1182/blood-2017-09-806398.

25. Hans CP, Weisenburger DD, Greiner TC, Gascoyne RD, Delabie J, Ott G, Müller-Hermelink HK, Campo E, Braziel RM, Jaffe ES, Pan Z, Farinha P, Smith LM, Falini B, Banham AH, Rosenwald A, Staudt LM, Connors JM, Armitage JO, Chan WC. Confirmation of the molecular classification of diffuse large B-cell lymphoma by immunohistochemistry using a tissue microarray. Blood. 2004 Jan 1;103(1):275-82. doi: 10.1182/blood-2003-05-1545.

26. Hav M, Gerdtsson E, Singh M, Colombo A, Hicks J, Kuhn P, Siddiqi I, Merchant A. Abstract 2789: Highly multiplexed imaging mass cytometry reveals immune cell composition and spatial heterogeneity in diffuse large B cell lymphoma associated with treatment outcome. Cancer Res 2019;79:2789.

27. Hossain NM, Dahiya S, Le R, Abramian AM, Kong KA, Muffly LS, Miklos DB. Circulating tumor DNA assessment in patients with diffuse large B-cell lymphoma following CAR T-cell therapy. Leuk Lymphoma. 2019 Feb;60(2):503-506. doi: 10.1080/10428194.2018.1474463.

28. Huet S, Salles G. Potential of Circulating Tumor DNA for the Management of Patients With Lymphoma. JCO Oncol Pract. 2020 Sep;16(9):561-568. doi: 10.1200/JOP.19.00691.

29. Huntington SF, Svoboda J, Doshi JA. Cost-effectiveness analysis of routine surveillance imaging of patients with diffuse large B-cell lymphoma in first remission. J Clin Oncol. 2015 May 1;33(13):1467-74. doi: 10.1200/JCO.2014.58.5729.

30. International Non-Hodgkin's Lymphoma Prognostic Factors Project. A predictive model for aggressive non-Hodgkin's lymphoma. N Engl J Med. 1993 Sep 30;329(14):987-94. doi: 10.1056/NEJM199309303291402.

31. Jiang Y, Nie K, Redmond D, Melnick AM, Tam W, Elemento O. VDJ-Seq: Deep Sequencing Analysis of Rearranged Immunoglobulin Heavy Chain Gene to Reveal Clonal Evolution Patterns of B Cell Lymphoma. J Vis Exp. 2015 Dec 28;(106):e53215. doi: 10.3791/53215.

32. Kanas G, Ge W, Quek RGW, Keeven K, Nersesyan K, Jon E Arnason. Epidemiology of diffuse large B-cell lymphoma (DLBCL) and follicular lymphoma (FL) in the United States and Western Europe: population-level projections for 2020-2025. Leuk Lymphoma. 2022 Jan;63(1):54-63. doi: 10.1080/10428194.2021.

33. Kurtz DM, Esfahani MS, Scherer F, Soo J, Jin MC, Liu CL, Newman AM, Dührsen U, Hüttmann A, Casasnovas O, Westin JR, Ritgen M, Böttcher S, Langerak AW, Roschewski M, Wilson WH, Gaidano G, Rossi D, Bahlo J, Hallek M, Tibshirani R, Diehn M, Alizadeh AA. Dynamic Risk Profiling Using Serial Tumor Biomarkers for Personalized Outcome Prediction. Cell. 2019 Jul 25;178(3):699-713.e19. doi: 10.1016/j.cell.2019.06.011.

34. Kurtz DM, Green MR, Bratman SV, Scherer F, Liu CL, Kunder CA, Takahashi K, Glover C, Keane C, Kihira S, Visser B, Callahan J, Kong KA, Faham M, Corbelli KS, Miklos D, Advani RH, Levy R, Hicks RJ, Hertzberg M, Ohgami RS, Gandhi MK, Diehn M, Alizadeh AA. Noninvasive monitoring of diffuse large B-cell lymphoma by immunoglobulin high-throughput sequencing. Blood. 2015 Jun 11;125(24):3679-87. doi: 10.1182/blood-2015-03-635169.

35. Kurtz DM, Scherer F, Jin MC, Soo J, Craig AFM, Esfahani MS, Chabon JJ, Stehr H, Liu CL, Tibshirani R, Maeda LS, Gupta NK, Khodadoust MS, Advani RH, Levy R, Newman AM, Dührsen U, Hüttmann A, Meignan M, Casasnovas RO, Westin JR, Roschewski M, Wilson

WH, Gaidano G, Rossi D, Diehn M, Alizadeh AA. Circulating Tumor DNA Measurements As Early Outcome Predictors in Diffuse Large B-Cell Lymphoma. J Clin Oncol. 2018 Oct 1;36(28):2845-2853. doi: 10.1200/JCO.2018.78.5246.

36. Kurtz DM, Soo J, Co Ting Keh L, Alig S, Chabon JJ, Sworder BJ, Schultz A, Jin MC, Scherer F, Garofalo A, Macaulay CW, Hamilton EG, Chen B, Olsen M, Schroers-Martin JG, Craig AFM, Moding EJ, Esfahani MS, Liu CL, Dührsen U, Hüttmann A, Casasnovas RO, Westin JR, Roschewski M, Wilson WH, Gaidano G, Rossi D, Diehn M, Alizadeh AA. Enhanced detection of minimal residual disease by targeted sequencing of phased variants in circulating tumor DNA. Nat Biotechnol. 2021 Dec;39(12):1537-1547. doi: 10.1038/s41587-021-00981-w.

37. Lakhotia R, Roschewski M. Circulating tumour DNA in B-cell lymphomas: current state and future prospects. Br J Haematol. 2021 Jun;193(5):867-881. doi: 10.1111/bjh.17251.

38. Landgren, O, Rustad, EH. Meeting report: Advances in minimal residual disease testing in multiple myeloma 2018. Adv Cell Gene Ther. 2019; 2:e26. https://doi.org/10.1002/acg2.26

39. Lauer EM, Mutter J, Scherer F. Circulating tumor DNA in B-cell lymphoma: technical advances, clinical applications, and perspectives for translational research. Leukemia. 2022 Sep;36(9):2151-2164. doi: 10.1038/s41375-022-01618-w.

40. Mamot C, Klingbiel D, Hitz F, Renner C, Pabst T, Driessen C, Mey U, Pless M, Bargetzi M, Krasniqi F, Gigli F, Hany T, Samarin A, Biaggi C, Rusterholz C, Dirnhofer S, Zucca E, Martinelli G. Final Results of a Prospective Evaluation of the Predictive Value of Interim Positron Emission Tomography in Patients With Diffuse Large B-Cell Lymphoma Treated With R-CHOP-14 (SAKK 38/07). J Clin Oncol. 2015 Aug 10;33(23):2523-9. doi: 10.1200/JCO.2014.58.9846.

41. Maurer MJ, Ghesquières H, Jais JP, Witzig TE, Haioun C, Thompson CA, Delarue R, Micallef IN, Peyrade F, Macon WR, Jo Molina T, Ketterer N, Syrbu SI, Fitoussi O, Kurtin PJ, Allmer C, Nicolas-Virelizier E, Slager SL, Habermann TM, Link BK, Salles G, Tilly H, Cerhan JR. Event-free survival at 24 months is a robust end point for disease-related outcome in diffuse large B-cell lymphoma treated with immunochemotherapy. J Clin Oncol. 2014 Apr 1;32(10):1066-73. doi: 10.1200/JCO.2013.51.5866.

42. McKelvey EM, Gottlieb JA, Wilson HE, Haut A, Talley RW, Stephens R, Lane M, Gamble JF, Jones SE, Grozea PN, Gutterman J, Coltman C, Moon TE. Hydroxyldaunomycin (Adriamycin) combination chemotherapy in malignant lymphoma. Cancer. 1976

Oct;38(4):1484-93. doi: 10.1002/1097-0142(197610)38:4<1484::aid-cncr2820380407>3.0.co;2-i.

43. Melani C, Wilson WH, Roschewski M. Liquid biopsy in non-Hodgkin's lymphoma. Hematol Oncol. 2019 Jun;37 Suppl 1:70-74. doi: 10.1002/hon.2587.

44. Meriranta L, Alkodsi A, Pasanen A, Lepistö M, Mapar P, Blaker YN, Jørgensen J, Karjalainen-Lindsberg ML, Fiskvik I, Mikalsen LTG, Autio M, Björkholm M, Jerkeman M, Fluge Ø, Brown P, Jyrkkiö S, Holte H, Pitkänen E, Ellonen P, Leppä S. Molecular features encoded in the ctDNA reveal heterogeneity and predict outcome in high-risk aggressive B-cell lymphoma. Blood. 2022 Mar 24;139(12):1863-1877. doi: 10.1182/blood.2021012852.

45. Merryman RW, Redd RA,Taranto E, Ahmed G, Jeter E, McHugh KM, Brown JR, Crombie J, Davids MS, Fisher DC, Freedman AS, Jacobsen E, Jacobson C, Kim AI, LaCasce AS, Lampson BL, Samuel Ng, Odejide OO, Dahi PB, Nieto Y, Joyce RM, Chen YB, Herrera AF, Armand P. Prognostic Value of Circulating Tumor DNA (ctDNA) in Autologous Stem Cell Graft and Post-Transplant Plasma Samples Among Patients with Diffuse Large B-Cell Lymphoma. Blood 2020; 136 (Supplement 1): 22–23. doi: https://doi.org/10.1182/blood-2020-140965

46. Moghbel MC, Mittra E, Gallamini A, Niederkohr R, Chen DL, Zukotynski K, Nadel H, Kostakoglu L. Response Assessment Criteria and Their Applications in Lymphoma: Part 2. J Nucl Med. 2017 Jan;58(1):13-22. doi: 10.2967/jnumed.116.184242.

47. Nowakowski GS, Czuczman MS. ABC, GCB, and Double-Hit Diffuse Large B-Cell Lymphoma: Does Subtype Make a Difference in Therapy Selection? Am Soc Clin Oncol Educ Book. 2015:e449-57. doi: 10.14694/EdBook_AM.2015.35.e449.

48. Pasqualucci L, Dalla-Favera R. The genetic landscape of diffuse large B-cell lymphoma. Semin Hematol. 2015 Apr;52(2):67-76. doi: 10.1053/j.seminhematol.2015.01.005.

49. Pirosa MC, Borchmann S, Jardin F, Gaidano G, Rossi D. Controversies in the Interpretation of Liquid Biopsy Data in Lymphoma. Hemasphere. 2022 May 13;6(6):e727. doi: 10.1097/HS9.0000000000000727.

50. Poynton E, Okosun J. Liquid biopsy in lymphoma: is it primed for clinical translation? eJHaem. 2021; 2: 616– 27.

51. Pregno P, Chiappella A, Bellò M, Botto B, Ferrero S, Franceschetti S, Giunta F, Ladetto M, Limerutti G, Menga M, Nicolosi M, Priolo G, Puccini B, Rigacci L, Salvi F, Vaggelli L,

Passera R, Bisi G, Vitolo U. Interim 18-FDG-PET/CT failed to predict the outcome in diffuse large B-cell lymphoma patients treated at the diagnosis with rituximab-CHOP. Blood. 2012 Mar 1;119(9):2066-73. doi: 10.1182/blood-2011-06-359943.

52. Rajewsky K. Clonal selection and learning in the antibody system. Nature. 1996 Jun 27;381(6585):751-8. doi: 10.1038/381751a0.

53. Roschewski M, Dunleavy K, Pittaluga S, Moorhead M, Pepin F, Kong K, Shovlin M, Jaffe ES, Staudt LM, Lai C, Steinberg SM, Chen CC, Zheng J, Willis TD, Faham M, Wilson WH. Circulating tumour DNA and CT monitoring in patients with untreated diffuse large B-cell lymphoma: a correlative biomarker study. Lancet Oncol. 2015 May;16(5):541-9. doi: 10.1016/S1470-2045(15)70106-3.

54. Roschewski M, Rossi D, Kurtz DM, Alizadeh AA, Wilson WH. Circulating Tumor DNA in Lymphoma: Principles and Future Directions. Blood Cancer Discov. 2022 Jan;3(1):5-15. doi: 10.1158/2643-3230.BCD-21-0029.

55. Roschewski M, Staudt LM, Wilson WH. Diffuse large B-cell lymphoma-treatment approaches in the molecular era. Nat Rev Clin Oncol. 2014 Jan;11(1):12-23. doi: 10.1038/nrclinonc.2013.197.

56. Roschewski M, Staudt LM, Wilson WH. Dynamic monitoring of circulating tumor DNA in non-Hodgkin lymphoma. Blood. 2016 Jun 23;127(25):3127-32. doi: 10.1182/blood-2016-03-635219. Epub 2016 Apr 14.

57. Rosenwald A, Bens S, Advani R, Barrans S, Copie-Bergman C, Elsensohn MH, Natkunam Y, Calaminici M, Sander B, Baia M, Smith A, Painter D, Pham L, Zhao S, Ziepert M, Jordanova ES, Molina TJ, Kersten MJ, Kimby E, Klapper W, Raemaekers J, Schmitz N, Jardin F, Stevens WBC, Hoster E, Hagenbeek A, Gribben JG, Siebert R, Gascoyne RD, Scott DW, Gaulard P, Salles G, Burton C, de Jong D, Sehn LH, Maucort-Boulch D. Prognostic Significance of MYC Rearrangement and Translocation Partner in Diffuse Large B-Cell Lymphoma: A Study by the Lunenburg Lymphoma Biomarker Consortium. J Clin Oncol. 2019 Dec 10;37(35):3359-3368. doi: 10.1200/JCO.19.00743.

58. Rosenwald A, Wright G, Chan WC, Connors JM, Campo E, Fisher RI, Gascoyne RD, Muller-Hermelink HK, Smeland EB, Giltnane JM, Hurt EM, Zhao H, Averett L, Yang L, Wilson WH, Jaffe ES, Simon R, Klausner RD, Powell J, Duffey PL, Longo DL, Greiner TC, Weisenburger DD, Sanger WG, Dave BJ, Lynch JC, Vose J, Armitage JO, Montserrat E, López-Guillermo A, Grogan TM, Miller TP, LeBlanc M, Ott G, Kvaloy S, Delabie J, Holte

H, Krajci P, Stokke T, Staudt LM; Lymphoma/Leukemia Molecular Profiling Project. The use of molecular profiling to predict survival after chemotherapy for diffuse large-B-cell lymphoma. N Engl J Med. 2002 Jun 20;346(25):1937-47. doi: 10.1056/NEJMoa012914.

59. Rossi D, Diop F, Spaccarotella E, Monti S, Zanni M, Rasi S, Deambrogi C, Spina V, Bruscaggin A, Favini C, Serra R, Ramponi A, Boldorini R, Foà R, Gaidano G. Diffuse large B-cell lymphoma genotyping on the liquid biopsy. Blood. 2017 Apr 6;129(14):1947-1957. doi: 10.1182/blood-2016-05-719641.

60. Rossi D, Spina V, Bruscaggin A, Gaidano G. Liquid biopsy in lymphoma. Haematologica. 2019 Apr;104(4):648-652. doi: 10.3324/haematol.2018.206177.

61. Ruppert AS, Dixon JG, Salles G, Wall A, Cunningham D, Poeschel V, Haioun C, Tilly H, Ghesquieres H, Ziepert M, Flament J, Flowers C, Shi Q, Schmitz N. International prognostic indices in diffuse large B-cell lymphoma: a comparison of IPI, R-IPI, and NCCN-IPI. Blood. 2020 Jun 4;135(23):2041-2048. doi: 10.1182/blood.2019002729.

62. Rushton CK, Arthur SE, Alcaide M, Cheung M, Jiang A, Coyle KM, Cleary KLS, Thomas N, Hilton LK, Michaud N, Daigle S, Davidson J, Bushell K, Yu S, Rys RN, Jain M, Shepherd L, Marra MA, Kuruvilla J, Crump M, Mann K, Assouline S, Connors JM, Steidl C, Cragg MS, Scott DW, Johnson NA, Morin RD. Genetic and evolutionary patterns of treatment resistance in relapsed B-cell lymphoma. Blood Adv. 2020 Jul 14;4(13):2886-2898. doi: 10.1182/bloodadvances.2020001696.

63. Sapkota S, Shaikh H. Non-Hodgkin Lymphoma [Updated 2022 May 1]. StatPearls Publishing; 2022 Jan-. Available from: https://www.ncbi.nlm.nih.gov/books/NBK559328/

64. Savage KJ, Johnson NA, Ben-Neriah S, Connors JM, Sehn LH, Farinha P, Horsman DE, Gascoyne RD. MYC gene rearrangements are associated with a poor prognosis in diffuse large B-cell lymphoma patients treated with R-CHOP chemotherapy. Blood. 2009 Oct 22;114(17):3533-7. doi: 10.1182/blood-2009-05-220095.

65. Scheijen B, Meijers RWJ, Rijntjes J, van der Klift MY, Möbs M, Steinhilber J, Reigl T, van den Brand M, Kotrová M, Ritter JM, Catherwood MA, Stamatopoulos K, Brüggemann M, Davi F, Darzentas N, Pott C, Fend F, Hummel M, Langerak AW, Groenen PJTA; EuroClonality-NGS Working Group. Next-generation sequencing of immunoglobulin gene rearrangements for clonality assessment: a technical feasibility study by EuroClonality-NGS. Leukemia. 2019 Sep;33(9):2227-2240. doi: 10.1038/s41375-019-0508-7.

66. Scherer F, Kurtz DM, Diehn M, Alizadeh AA. High-throughput sequencing for noninvasive disease detection in hematologic malignancies. Blood. 2017 Jul 27;130(4):440-452. doi: 10.1182/blood-2017-03-735639.

67. Scherer F, Kurtz DM, Newman AM, Stehr H, Craig AF, Esfahani MS, Lovejoy AF, Chabon JJ, Klass DM, Liu CL, Zhou L, Glover C, Visser BC, Poultsides GA, Advani RH, Maeda LS, Gupta NK, Levy R, Ohgami RS, Kunder CA, Diehn M, Alizadeh AA. Distinct biological subtypes and patterns of genome evolution in lymphoma revealed by circulating tumor DNA. Sci Transl Med. 2016 Nov 9;8(364):364ra155. doi: 10.1126/scitranslmed.aai8545.

68. Schmitz R, Wright GW, Huang DW, Johnson CA, Phelan JD, Wang JQ, Roulland S, Kasbekar M, Young RM, Shaffer AL, Hodson DJ, Xiao W, Yu X, Yang Y, Zhao H, Xu W, Liu X, Zhou B, Du W, Chan WC, Jaffe ES, Gascoyne RD, Connors JM, Campo E, Lopez-Guillermo A, Rosenwald A, Ott G, Delabie J, Rimsza LM, Tay Kuang Wei K, Zelenetz AD, Leonard JP, Bartlett NL, Tran B, Shetty J, Zhao Y, Soppet DR, Pittaluga S, Wilson WH, Staudt LM. Genetics and Pathogenesis of Diffuse Large B-Cell Lymphoma. N Engl J Med. 2018 Apr 12;378(15):1396-1407. doi: 10.1056/NEJMoa1801445.

69. Sehn LH, Donaldson J, Chhanabhai M, Fitzgerald C, Gill K, Klasa R, MacPherson N, O'Reilly S, Spinelli JJ, Sutherland J, Wilson KS, Gascoyne RD, Connors JM. Introduction of combined CHOP plus rituximab therapy dramatically improved outcome of diffuse large B-cell lymphoma in British Columbia. J Clin Oncol. 2005 Aug 1;23(22):5027-33. doi: 10.1200/JCO.2005.09.137.

70. Sehn LH, Salles G. Diffuse Large B-Cell Lymphoma. N Engl J Med. 2021 Mar 4;384(9):842-858. doi: 10.1056/NEJMra2027612.

71. Soscia R, Della Starza I, De Novi LA, Ilari C, Ansuinelli M, Cavalli M, Bellomarino V, Cafforio L, Di Trani M, Cazzaniga G, Fazio G, Santoro A, Salemi D, Spinelli O, Tosi M, Terragna C, Robustelli V, Bellissimo T, Colafigli G, Breccia M, Chiaretti S, Di Rocco A, Martelli M, Guarini A, Del Giudice I, Foà R. Circulating cell-free DNA for target quantification in hematologic malignancies: Validation of a protocol to overcome pre-analytical biases. Hematol Oncol. 2023 Feb;41(1):50-60. doi: 10.1002/hon.3087.

72. Spina V, Bruscaggin A, Cuccaro A, Martini M, Di Trani M, Forestieri G, Manzoni M, Condoluci A, Arribas A, Terzi-Di-Bergamo L, Locatelli SL, Cupelli E, Ceriani L, Moccia AA, Stathis A, Nassi L, Deambrogi C, Diop F, Guidetti F, Cocomazzi A, Annunziata S, Rufini V, Giordano A, Neri A, Boldorini R, Gerber B, Bertoni F, Ghielmini M, Stüssi G, Santoro A,

Cavalli F, Zucca E, Larocca LM, Gaidano G, Hohaus S, Carlo-Stella C, Rossi D. Circulating tumor DNA reveals genetics, clonal evolution, and residual disease in classical Hodgkin lymphoma. Blood. 2018 May 31;131(22):2413-2425. doi: 10.1182/blood-2017-11-812073.

73. Susanibar-Adaniya S, Barta SK. 2021 Update on Diffuse large B cell lymphoma: A review of current data and potential applications on risk stratification and management. Am J Hematol. 2021 May 1;96(5):617-629. doi: 10.1002/ajh.26151.

74. Swerdlow SH, Campo E, Pileri SA, Harris NL, Stein H, Siebert R, Advani R, Ghielmini M, Salles GA, Zelenetz AD, Jaffe ES. The 2016 revision of the World Health Organization classification of lymphoid neoplasms. Blood. 2016 May 19;127(20):2375-90. doi: 10.1182/blood-2016-01-643569.

75. Sworder B, Kurtz DM, Alig S, Frank MJ, Macauley CW, Garofalo A, Shukla N, Sahaf B, Esfahani MS, Sheybani N, Schroers-Martin J, Liu CL, Olsen M, Spiegel JY, Oak J, Jin MC, Beygi S, Khodadoust MS, Natkunam Y, Majzner R, Mackall CL, Diehn M, Miklos DM and Alizadeh AA. Determinants of resistance to engineered T-cell therapies targeting CD19 in lymphoma. Hematol Oncol. 2021;39. doi: https://doi.org/10.1002/hon.6_2879

76. Thompson CA, Ghesquieres H, Maurer MJ, Cerhan JR, Biron P, Ansell SM, Chassagne-Clément C, Inwards DJ, Gargi T, Johnston PB, Nicolas-Virelizier E, Macon WR, Peix M, Micallef IN, Sebban C, Nowakowski GS, Porrata LF, Weiner GJ, Witzig TE, Habermann TM, Link BK. Utility of routine post-therapy surveillance imaging in diffuse large B-cell lymphoma. J Clin Oncol. 2014 Nov 1;32(31):3506-12. doi: 10.1200/JCO.2014.55.7561.

77. Tilly H, Gomes da Silva M, Vitolo U, Jack A, Meignan M, Lopez-Guillermo A, Walewski J, André M, Johnson PW, Pfreundschuh M, Ladetto M; ESMO Guidelines Committee. Diffuse large B-cell lymphoma (DLBCL): ESMO Clinical Practice Guidelines for diagnosis, treatment and follow-up. Ann Oncol. 2015 Sep;26 Suppl 5:v116-25. doi: 10.1093/annonc/mdv304.

78. Wright GW, Huang DW, Phelan JD, Coulibaly ZA, Roulland S, Young RM, Wang JQ, Schmitz R, Morin RD, Tang J, Jiang A, Bagaev A, Plotnikova O, Kotlov N, Johnson CA, Wilson WH, Scott DW, Staudt LM. A Probabilistic Classification Tool for Genetic Subtypes of Diffuse Large B Cell Lymphoma with Therapeutic Implications. Cancer Cell. 2020 Apr 13;37(4):551-568.e14. doi: 10.1016/j.ccell.2020.03.015.

79. Zelenetz AD, Abramson JS, Advani RH, Andreadis CB, Bartlett N, Bellam N, Byrd JC, Czuczman MS, Fayad LE, Glenn MJ, Gockerman JP, Gordon LI, Harris NL, Hoppe RT,

Horwitz SM, Kelsey CR, Kim YH, LaCasce AS, Nademanee A, Porcu P, Press O, Pro B, Reddy N, Sokol L, Swinnen LJ, Tsien C, Vose JM, Wierda WG, Yahalom J, Zafar N. Non-Hodgkin's lymphomas. J Natl Compr Canc Netw. 2011 May;9(5):484-560. doi: 10.6004/jnccn.2011.0046. PMID: 21550968.

80. Zhou Z, Sehn LH, Rademaker AW, Gordon LI, Lacasce AS, Crosby-Thompson A, Vanderplas A, Zelenetz AD, Abel GA, Rodriguez MA, Nademanee A, Kaminski MS, Czuczman MS, Millenson M, Niland J, Gascoyne RD, Connors JM, Friedberg JW, Winter JN. An enhanced International Prognostic Index (NCCN-IPI) for patients with diffuse large B-cell lymphoma treated in the rituximab era. Blood. 2014 Feb 6;123(6):837-42. doi: 10.1182/blood-2013-09-524108.

81. Ziepert M, Hasenclever D, Kuhnt E, Glass B, Schmitz N, Pfreundschuh M, Loeffler M. Standard International prognostic index remains a valid predictor of outcome for patients with aggressive CD20+ B-cell lymphoma in the rituximab era. J Clin Oncol. 2010 May 10;28(14):2373-80. doi: 10.1200/JCO.2009.26.2493.